Journal of Structural Geology 199 (2025) 105495

Contents lists available at ScienceDirect

Journal of Structural Geology

journal homepage: www.elsevier.com/locate/jsg

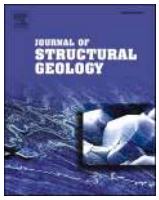

Invited Research Article

Deformation and magnetic fabrics in isoclinal folds of the Variscan Pyrenees

B. Oliva-Urcia [a,*], T. Román-Berdiel [a], P. Clariana [b], R. Soto [b], E. Izquierdo-Llavall [b], A. Casas-Sainz [a]

[a] Geodinámica Interna (Geotransfer-IUCA), Departamento de Ciencias de La Tierra, Universidad de Zaragoza, 50009, Zaragoza, Spain
[b] Instituto Geológico y Minero de España, CSIC, Unidad de Zaragoza, 50059, Zaragoza, Spain

ARTICLE INFO

Keywords:
Anisotropy of magnetic susceptibility
Limestones
Isocline folds
Variscan
Alpine
Pyrenees

ABSTRACT

Magnetic fabrics are used as strain markers since they reflect the orientation-distribution of grains in a rock. In this work we analyzed, from the point of view of anisotropy of magnetic susceptibility (at low-temperature and room temperature), Devonian (29 sites) and Ordovician-Silurian (3 sites) sedimentary rocks in the Pyrenean Axial Zone, totalling 611 samples. The main target is to determine the strain in relation to the Variscan (polyphased) and Alpine orogenies in limestones and shales. The magnetic information also derives from thermomagnetic curves, acquisition of the isothermal remanent magnetization (IRM) and coercivity of the remanence analyses, together with hysteresis loops and stepwise thermal demagnetization of induced IRM in 3 axes techniques. The analyses of magnetic properties were complemented with optical microscopy observations and calcimetries. In two of the sample areas (Sen and Llisat valleys), the minimum axes of the magnetic susceptibility ellipsoid (k_{min} axes) are mostly perpendicular to bedding whereas in the other two (Zinqueta valley and near Posets peak area), a more developed tectonic fabric is found: the k_{min} axes are not completely perpendicular to bedding, and the magnetic susceptibility ellipsoid relates to the foliation plane. Different minerals carry a concordant magnetic fabric with pyrrhotite, magnetite (ferromagnetic *s.l.*) and phyllosilicates (paramagnetic), and little influence of calcite grains (diamagnetic). The magnetic fabric is interpreted to form at the early stages of the Variscan deformation, prior to the dextral transpression synchronous with granite emplacement that characterizes the late stages of the Variscan Orogeny. However, contact metamorphism and associated fluid circulation can enhance or obliterate the primary magnetic fabric.

1. Introduction

The analyses of magnetic fabrics are performed to decipher deformation in rocks. The anisotropy of the magnetic susceptibility (AMS) is a technique that has been used in all types of rocks since the discovery of the anisotropic behavior of the magnetic susceptibility (Graham, 1966), and it is of particular interest in sedimentary rocks from structural settings where the ductile component of deformation is cryptic (Parés, 2015). It is a method used in order to better understand the relationship between the magnetic signal of the anisotropy of the magnetic susceptibility (AMS) or magnetic fabric, and the tectonic imprint on folded rocks since it allows obtaining the orientation-distribution of grains (Mamtani and Sengupta, 2010; Hrouda and Chadima, 2020)). Therefore, AMS is found to be a sensitive indicator to describe the strain patterns at orogen-scale, particularly in areas with a modest degree of deformation (Pocoví-Juan et al., 2014). However, the superposition of different deformation events or the presence of different magnetic carriers can complicate a straightforward correlation. As pointed in Evans et al. (2003) and references therein, "All susceptibility fabrics are really composite fabrics". These authors refer to the term used by Housen et al. (1993) and consider magnetic fabrics as the result of the overprinting of i) a primary depositional magnetic fabric, ii) a diagenetic or compactional magnetic fabric and iii) a tectonic fabric (layer-parallel shortening prior to folding) (Evans et al., 2003).

In particular, the use of magnetic fabrics is discouraged as a strain gauge when composite magnetic fabrics are found (Debacker et al., 2004). However, composite magnetic fabrics potentially develop in, for example, tectonically inverted basins. They are pursued in order to

* Corresponding author.
E-mail addresses: boliva@unizar.es (B. Oliva-Urcia), mtdjrb@unizar.es (T. Román-Berdiel), p.clariana@igme.es (P. Clariana), r.soto@igme.es (R. Soto), e.izquierdo@igme.es (E. Izquierdo-Llavall), acasas@unizar.es (A. Casas-Sainz).

https://doi.org/10.1016/j.jsg.2025.105495
Received 3 March 2025; Received in revised form 17 June 2025; Accepted 25 June 2025
Available online 27 June 2025

disentangle the extensional direction at the time of formation of the basin and subsequent compressional deformation (García-Lasanta et al., 2018).

For the magnetic fabric to be understood when applied to deformed sedimentary rocks, it is a standard procedure to establish a relative dating with respect to the position of bedding. This allows to constrain the deformational history of the region. For the magnetic fabric, the orientation of the magnetic susceptibility ellipsoid axes has been described to evolve from (i) the "sedimentary type" of magnetic fabric, where the minimum (k_{min}) axes are perpendicular to the bedding plane and the intermediate (k_{int}) and the maximum (k_{max}) axes are scattered on the bedding plane, when no arrangement of particles due to paleo-currents is present at the time of sedimentation to (ii) a "tectonic type" magnetic fabric, with changes in the orientation of the magnetic lineation (clustering of the k_{max} axes) and foliation (plane perpendicular to the clustered k_{min} axes) (i.e., Parés et al., 1999). The scalar parameters of the ellipsoid such as the shape or the anisotropy of the magnetic susceptibility ellipsoid (AMS) also change (Boiron et al., 2020). The tectonic type fabric has also gradients (Parés et al., 1999). However, in compressional and extensional settings giving rise to foreland and extensional basins, a "tectonic type" will be the first magnetic fabric developed within the syntectonic sediments with the clustered magnetic lineation oriented perpendicular to compression or parallel to extension, respectively (García-Lasanta et al., 2018; Soto et al., 2022 and references therein, Fig. 1). This "tectonic type" occurs at the time of deposition of sediments under a specific tectonic framework. However, the most evolved magnetic fabric in foreland basins are found closer to the fold-and-thrust belt edifices, related to the tectonic foliation (cleavage)

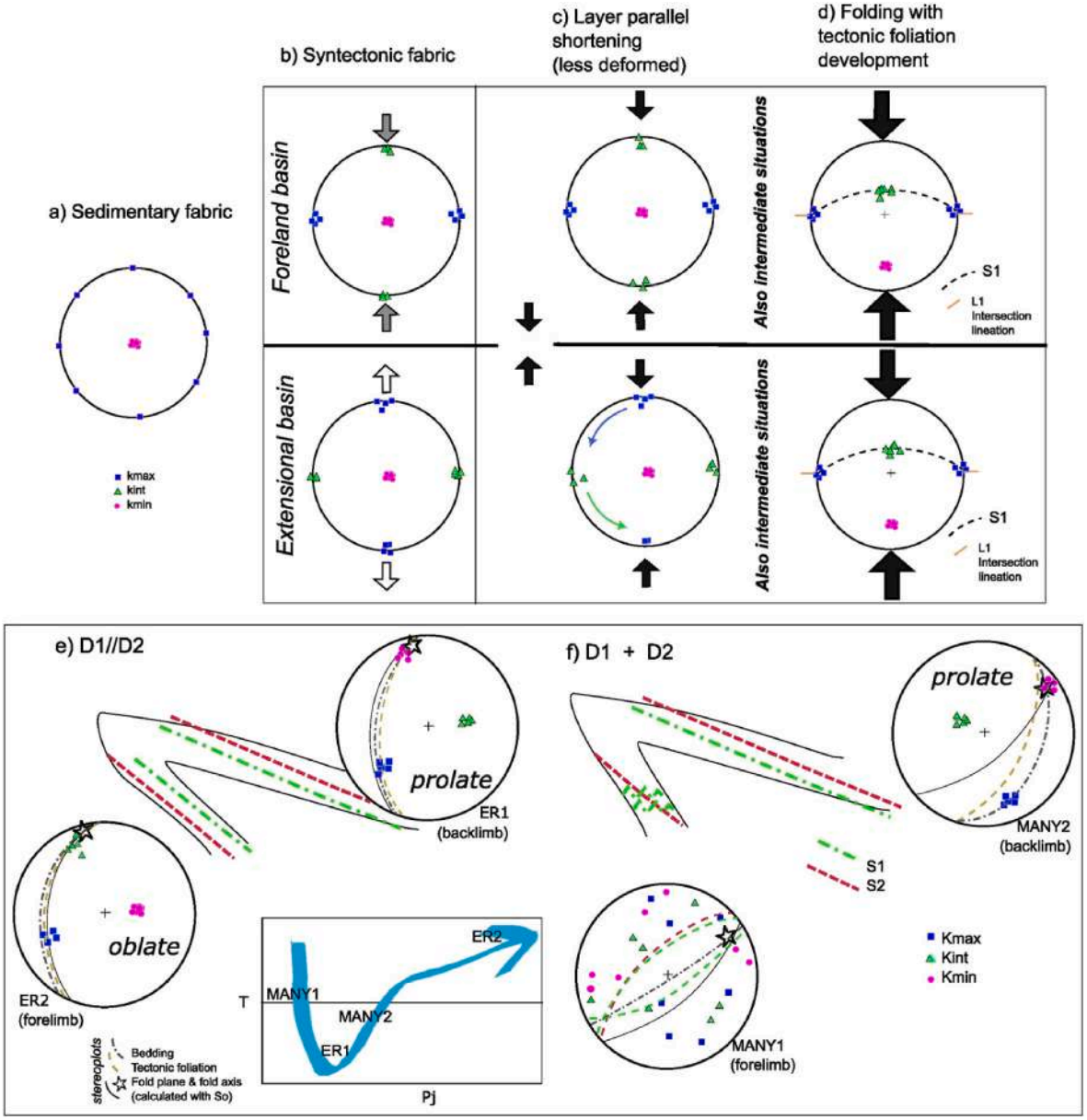

Fig. 1. a) to d) Stereoplot of magnetic fabric (k_{max} axes in blue, k_{int} axes in green, and k_{min} axes in pink) and its variation from sedimentary, syntectonic and to tectonic fabrics (layer parallel shortening and folded with tectonic foliation). The tectonic fabric can be divided in "early" (less deformed, layer parallel shortening) and later, more deformed folded rocks with tectonic foliation plane developed. Bedding plane is horizontal in all cases. e) and f) Magnetic fabric in Variscan folds with two phases of deformation (D1 with developed tectonic foliation S1 and D2 with developed tectonic foliation S2), in e) deduced apparent parallelism of deformational phases, f) deduced non parallelism of deformational phases (Oliva-Urcia et al., 2018). Variation of the shape (T) and corrected anisotropy degree (Pj) of the magnetic susceptibility ellipsoid (AMS) is shown for those particular sites. They follow the model by Parés et al. (1999). (For interpretation of the references to color in this figure legend, the reader is referred to the Web version of this article.)

plane, with k_{min} axes clustered on the pole to the cleavage plane, and k_{max} and k_{int} axes distributed within the cleavage plane after the inversion of the basin takes place. Therefore, depending on the relationship of the principal magnetic anisotropy directions and the principal directions of structural features (for example bedding or tectonic foliation), the term "normal" magnetic fabric is used when the magnetic lineation (k_{max} axes) is parallel to a structural lineation and the minimum axes (k_{min}) cluster perpendicularly to a structural foliation (i.e., bedding plane, tectonic foliation). The term "inverse" magnetic fabric is used when the maximum and minimum anisotropy axes are inverted relative to the normal fabric (Chadima et al., 2006). Other authors have definedsubtypes of inverse fabric (structural and magnetocrystalline) (Černý et al., 2020) but we will consider the relationship of the axes respect to the structural features solely. The term "inverse" fabric was described in rocks containing minerals with an inverse relationship between magnetic axes and shape and/or crystallographic axes (Rochette, 1988). The term "intermediate" fabric originated in models mixing normal and inverse fabric end-members but the axes still relate to the structural features (Chadima et al., 2006 and references therein). Finally, the term "anomalous" magnetic fabric will refer to a magnetic fabric with random distribution of magnetic axes respect to structural features (bedding or tectonic foliation) (Chadima et al., 2006 and references therein). Therefore, composite magnetic fabrics is a term that will describes the magnetic fabric developed during deformation, and it includes the magnetic fabrics that could show the orientation of the magnetic axes in unusual positions with respect to structural data ("anomalous" fabric). Composite fabrics can be "normal", "inverse" or "intermediate" fabrics, if the AMS axes relate to the structural features. (Averbuch et al., 1992; Chadima et al., 2006; Debacker et al., 2004; Graham, 1966; Jackson et al., 1989; Kissel et al., 1986; Oliva-Urcia et al., 2018; Parés et al., 1999; Pocoví-Juan et al., 2014; Soto et al., 2022 and references therein). The evolution model of magnetic fabrics in foreland basins was described by Parés et al. (1999), for extensional basins by Mattei et al. (1997) and for inverted sedimentary basins by García-Lasanta et al. (2018) and references therein.

In folds, generally, the tectonic magnetic fabric orients with the k_{max} axes parallel to the fold axis hinge provided that shortening is perpendicular to the fold axis, whereas the orientation of k_{min} axes may vary depending on the strain degree and the folding mechanism, i.e., development of cleavage, layer-parallel shortening, flexural flow, longitudinal straining and flattening. However, the magnetic fabric information is used to decipher the strain in a folded region when the k_{max} axes are not parallel to the fold axis, as for example in the Zagros belt where the k_{max} axes remain oriented according to a first stage of layer parallel shortening that is later folded in two stages (Aubourg et al., 2010). Magnetic fabric also records the tangential-longitudinal deformation in fold hinges and the flexural flow inferred for the fold limbs in syntectonic folds in the Pyrenees (Pueyo-Morer et al., 1997). It also has been used as complementary tool to decipher fold interference patterns in metamorphic rocks (Sayab et al., 2017), to distinguish tectonic phases (Raposo et al., 2014) or to describe the variation of the composite fabrics in multilayered folded systems where the tectonic inversion is stronger towards the orogen (Pueyo-Anchuela et al., 2010). The combination of magnetic fabrics with other magnetic (i.e., low temperature AMS, AARM), structural and petrographical analyses (i.e., paleostress analyses, quantification of deformation, calcite twinning, X-ray tomography …) helps disentangle the folding evolution at macro- and microscales (Mamtani and Sengupta, 2010; Sayab et al., 2017; Anastasio et al., 2016).

In addition, magnetic mineralogy can also affect the type of magnetic fabric, as it has been recognized in the folded marine platform rocks and the foreland basin rocks of the Pyrenees where paramagnetic fabric (mostly carried by phyllosilicates) and ferromagnetic fabric (mostly carried by magnetite, known by AARM) occur (Pueyo-Anchuela et al., 2010). For example, in limestones, the content of calcite can also have consequences for the results of magnetic fabric, since depending on the content of Fe and Mn in the calcite structure, crystals can change their magnetic behavior from diamagnetic to paramagnetic and they can also contain ferromagnetic inclusions (Schmidt et al., 2006).

In this work we present the magnetic fabric (AMS) and rock magnetism obtained in Paleozoic folded rocks (mostly Devonian carbonates and to less extent detrital Ordovician-Silurian rocks) from the Axial Zone of the Pyrenees. These folds formed during the Variscan Orogeny, for which different deformational phases have been described, and later, they were subsequently deformed by the Alpine Orogeny. In this scenario, the purposes of this work are (i) to discern and characterize the strain and ultimately, to contribute to the better understanding of the Variscan Orogeny in this sector of the Pyrenees and (ii) to check the limits of application of AMS in moderately deformed rocks having different lithologies.

2. Geological setting and sampling

The Pyrenean mountain range is described as a doubly vergent asymmetric orogen divided in five E-W trending structural zones: Northern Pyrenean Zone, Axial Zone, Southern Pyrenean Zone and the two foreland basins (Aquitanian and Ebro basins to the North and South respectively). This asymmetric orogen was formed by the Iberia-Europe convergence during Late Cretaceous-Miocene times. The Northern and Southern Zones are constituted by Mesozoic and Cenozoic deformed rocks whereas in the Axial Zone the Paleozoic basement crops out, forming the back-bone of the Range (Mattauer, 1968). The structure of the Axial Zone developed during the Alpine orogeny has been described as an antiformal stack (Muñoz, 1992) or imbricated thrust system with a dominant south vergence (Teixell, 1996; Martínez-Peña and Casas-Sainz, 2003) Fig. 2.

The general structure of the Axial Zone is mainly the result of polyphased Variscan deformation and to a lower extent, of Alpine deformation, whose influence, from the point of view of deformation, was more significant in the western Axial Zone (Choukroune and Séguret, 1973). Traditionally, two structural domains due to the Variscan structuring are described in the central and eastern part of the Axial Zone: infrastructure and suprastructure (Carreras and Capella, 1994; De Sitter and Zwart, 1960; Zwart, 1963). The infrastructure is characterized by a subhorizontal foliation developed under medium to high metamorphic grade, and the suprastructure is characterized by subvertical folds with associated axial planar foliation with very low to low metamorphic grade. The origin and geodynamic context of both structural units are still under debate. Nonetheless, the deformation and metamorphic grade increase from west to east in the Axial Zone. The intrusion of magmatic rocks occurred at the final stage of the Variscan Orogeny (late Carboniferous). The high-temperature processes in this Axial Zone of the Pyrenees, related to partial melting, gneiss dome formation and pluton emplacement occurred over a very short period, of the order of 5 Ma, at ~304 Ma (Denèle et al., 2014).

The Variscan structure in the studied area is located at the "intermediate" deformation zone, being affected a main deformation phase (D2) which coincides with (or postdate) granitoid emplacement (Gleizes et al., 1998). A prior D1 phase with fold and thrust development coincides with low-to-very-low grade (or absent) metamorphism (Carreras and Druget, 2014). These authors suggest that the granitoid emplacement, synchronous with the main deformational phase D2 in the internal more deformed zone, is post-tectonic in the intermediate zone, which is located towards the W of the Axial Zone. This idea contrasts with previous magnetic fabric studies in the granitoids of the central and western part of the Axial Zone, since they suggest a granitoid emplacement during dextral transpression related to the late Variscan deformation (Bouchez, 1997; Gleizes et al., 1998; Román-Berdiel et al., 2004, 2006).

Other authors, comparing the Axial Zone structures with the Alpine structures 60 km to the west of the study area (Anayet basin, Fig. 2a), found that the Variscan deformation created large scale recumbent folds vergent towards the west and with axial planar cleavage that were

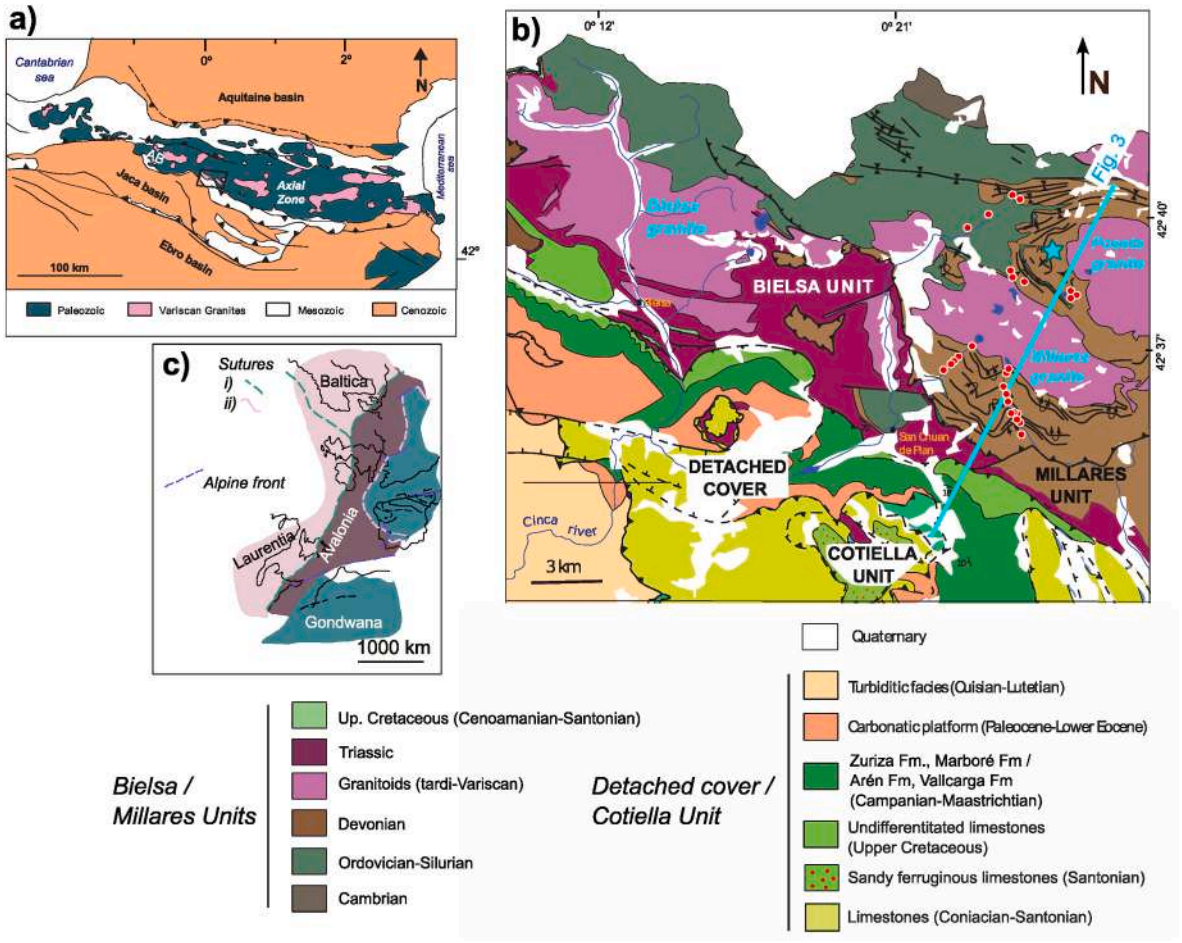

Fig. 2. a) Geological map of the Pyrenees (AB: Anayet basin), rectangle marks the study area (shown in b), b) geological map of the studied area, with the cross section of Fig. 3, the sampling locations (red dots) and the blue star that marks the Posets peak (just to the left of "Posets granite"). c) Simplified geological map of the Paleozoic orogenic belts at the end of Variscan convergence, sutures i) Rheic, ii) Iapetus-Tornquist. Green: Variscan belt, Dark purple: mostly Avalonian domain, Pink: mostly Caledonian-Acadian belts, modified from (Martínez-Catalán et al. (2009). Geology based on: IGME geologic maps, MAGNA series, map sheets numbers 147, 179 and 212. (For interpretation of the references to color in this figure legend, the reader is referred to the Web version of this article.)

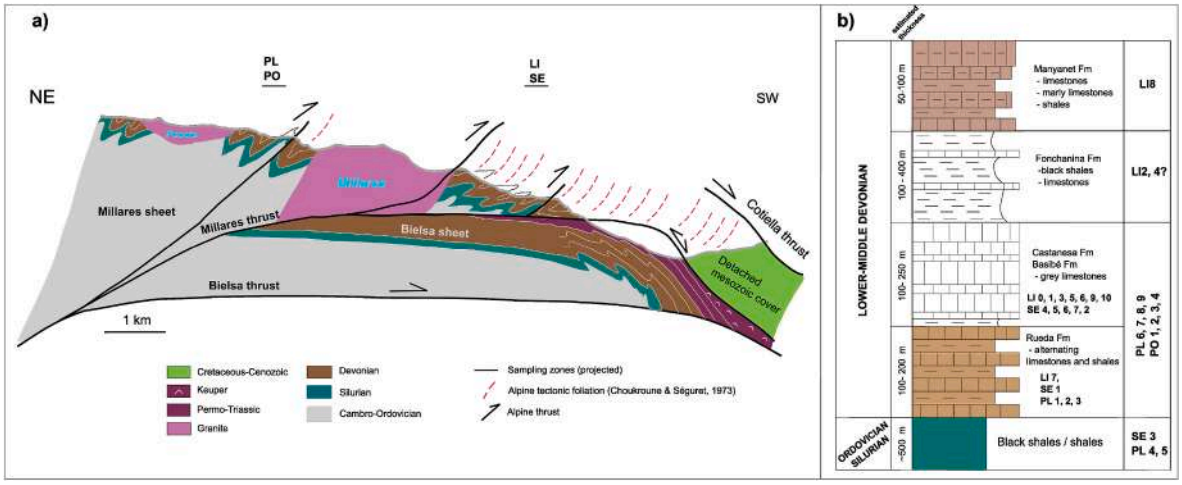

Fig. 3. a) General cross-section (simplified from Román-Berdiel et al., 2006), no vertical exaggeration. On top, the sampling zones projected (acronyms). 3. b) Simplified stratigraphic column with lithostratigraphic Lower Devonian formations (Mey, 1967) and position of the sampling sites. The information of the estimated thickness is from IGME geological maps (179, Bielsa).

subsequently deformed by an Alpine phase, giving Ramsay type 2 fold interference patterns of kilometric scale (Matte, 2002; Rodríguez-Méndez et al., 2013). In the Posets area, the fold interference pattern is described as type 3 but due to different phases of the Variscan Orogeny (Esteban et al., 2021). In any case, the main features observed in the studied area are recumbent folds vergent to the South associated

to foliation in the southern part: Sen and Llisat valleys, south of the Millares granite, and vertical folds and interference fold patterns (Grasemann et al., 2004) in the northern sector on Silurian and Devonian rocks (Posets area).

2.1. Stratigraphy

Most sites (29 out of 32) were sampled in Lower-Middle Devonian rocks and the other three sites were sampled in Ordovician-Silurian rocks (Fig. 3b). The Lower-Middle Devonian in the studied area is characterized by a succession of marine deposits from a shallow platform environment (García-Sansegundo, 1992), that show variations in thickness due to deformation. The different lithologies of the Devonian rocks were arranged in facies groups by Zwart (1979). The studied area is located in the "Sierra Negra" subarea, with a carbonatic part at the bottom and a silty part at the top that include, from bottom to top the Rueda, Castanesa, Fonchanina and Manyanet formationss (Lower-Middle Devonian) and the Vilaller Formation (Middle Devonian, Mey, 1967). The Ordovician-Silurian rocks in the studied area are mainly graptolitic black shales (and limestones in the upper part) (Zwart, 1979) that locally crop out close to thrust planes or at the hinge of anticlines.

2.2. Site location and geological structure

The recumbent kilometric folds with axial planar cleavage (namely S1) were sampled in the Llisat and Sen valleys, SE and SW of the Millares granite, respectively. These large scale folds can be clearly seen in orthophotographs, or for example in Google Earth. A total of 16 Devonian sites were sampled South of the Millares granite: 11 sites in the Llisat valley (acronym LI) and five sites in the Sen valley (acronym SE) plus one site in Silurian rocks in the Sen valley (SE-3). These two valleys, Llisat with N-S orientation and Sen with a NE-SW orientation are less than 3 km apart (Fig. 4a). The intersection lineation (L1) between the

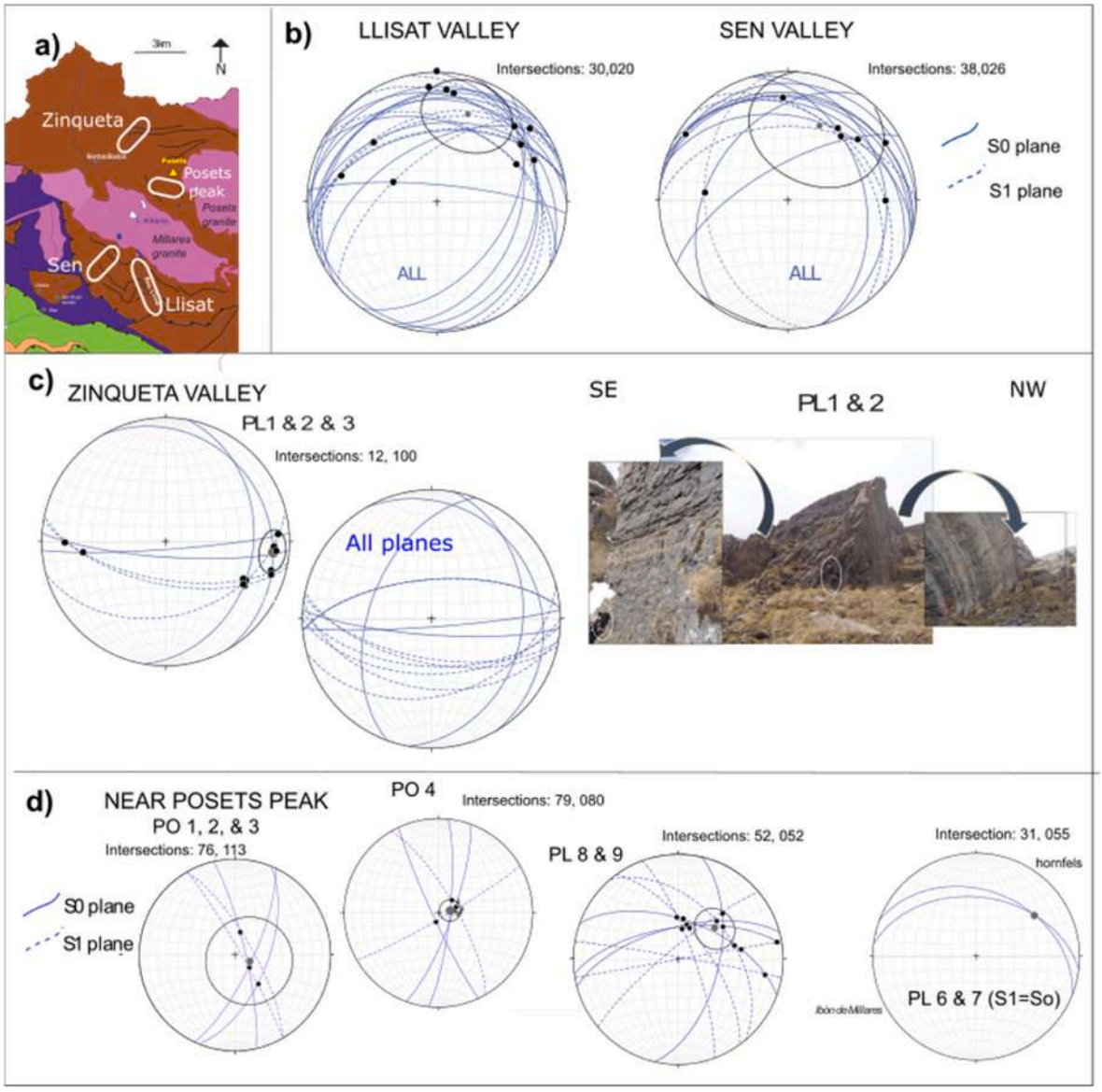

Fig. 4. a) Simplified geological map with ellipses marking the different sampling areas (Paleozoic rocks in brown, granites in pink, Triassic in blue and Cretaceous in green). Bedding (So) and cleavage data (S1) in stereographic projection (lower hemisphere) with the intersection lineation in b) Llisat and Sen valleys, c) Zinqueta valley area with field pictures oriented SE-NW, the ellipses mark human figures for scale, bedding/tectonic foliation is well observed, d) Posets peak area. The simplified geological cross-sections of these four areas are presented together with the magnetic fabric results in Figs. 10–13. (For interpretation of the references to color in this figure legend, the reader is referred to the Web version of this article.)

tectonic foliation (S1) and bedding (S0) in those sites has a NE orientation (N020E to N026E) plunging 30-38° N. Planes of S1 are subparallel to the S0 and can be interpreted as axial planar cleavage related to the recumbent folds (Fig. 4b).

In the Zinqueta valley, NW of the Millares granite and W of the Posets granite, three sites were sampled in Devonian rocks, and two sites in Ordovician-Silurian rocks. Here, a South-dipping, E-W tectonic foliation is well developed, and upright folds with South vergence are seen in outcrops close to the sampling sites (Fig. 4c). Near the Posets peak, eight sites were sampled in Devonian rocks, four sites (PL-6 to PL-9) just to the south of the thrust of Silurian over Devonian rocks and north of the Millares granite and four samples were collected in small scale folds to the west of the Posets granite (Fig. 4). The intersection lineation has different orientations and steeper plunge than in the previously described sites. The tectonic foliation is almost vertical with a NE-SW strike (Fig. 4d). Cleavage refraction due to lithological differences is observed in these outcrops (Fig. 5).

Contact metamorphism has a clear influence in a few sites: in the Llisat valley (LI-1), the Sen valley (SE-5) and North of the Millares granite (PL-6 and PL-7) where garnets (near PO) and andalusite crystals can be observed with the naked eye (in PL-6 and PL-7). The microscope observations confirm the presence of andalusite in some samples. Tension gashes perpendicular to bedding and with an E– orientation can also be observed in some outcrops.

2.3. Sampling strategy

A total of 47 oriented hand samples distributed in 32 sites were taken in two protected areas after permits were issued, in the Sobrarbe Pirineos UNESCO Global Geopark (European *Geopark* Network) and in the Posets-Maladeta Natural Park (Aragón Government, INAGA). This sampling method was selected to avoid noise, possible fumes and oil

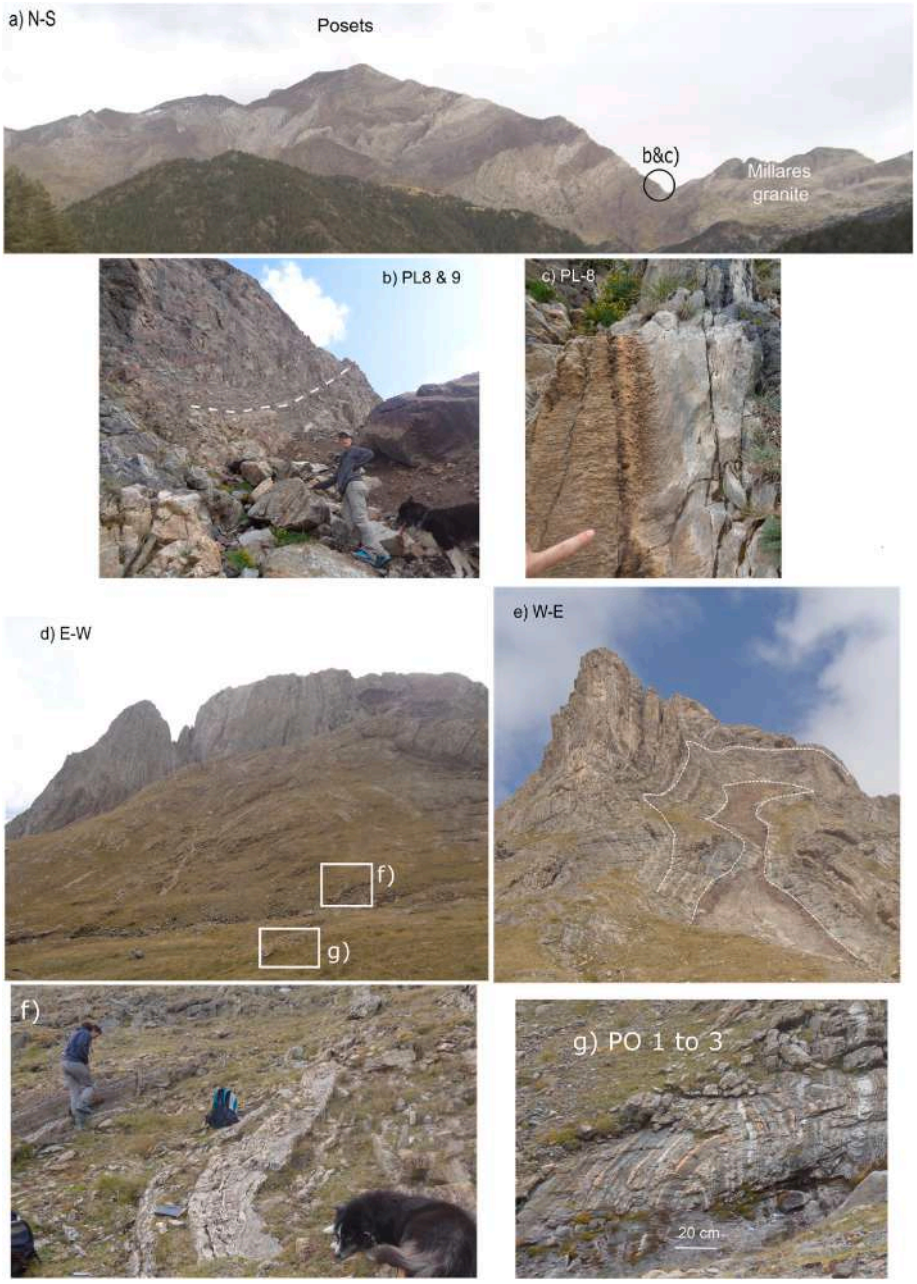

Fig. 5. Field pictures of folds a, d and e) to the S and SW of the Posets peak (north of Millares granite) and different zooming in b) PL-9 and c) PL-8 with cleavage refraction. In d) the location of f) and g) is shown and a basic dyke that cuts across the Variscan folds (visible on the center-left).

pollution of the drill machine. In addition, hand samples were taken at out of sight places to avoid visual contamination (as suggested by the GeoPark managers in the "sampling etiquette leaflet" https://www.geoparquepirineos.com/descargas/folleto_geoconservacion_cientifico_r.pdf).

From the hand samples, 611 standard specimens were cut in cubes of ~8 cm^3 that are distributed as follows: 202 specimens correspond to four folds in the Zinqueta and Posets areas, 210 specimens correspond to six folds in the LIisat valley and 199 specimens correspond to three folds in the Sen valley, see Figs. 2–5.

3. Methodology

The anisotropy of the magnetic susceptibility (AMS) was analyzed at room temperature at the Laboratory of Magnetic Fabrics of the University of Zaragoza (Geotransfer Group-IUCA, Spain). The AMS is a second rank tensor represented by an ellipsoid with three axes ($k_{max} \geq k_{int} \geq k_{min}$). The measurements in the KLY3 (AGICO Inc.) at 875 Hz frequency and 300 A/m field intensity, provide scalar values related to the AMS: bulk magnetic susceptibility (Km), the average of the ratio between induced magnetization (M) and applied magnetic field (H) of the samples in one site, the shape parameter T (values from 1 to 0 are oblate ellipsoids and from 0 to −1 are prolate ellipsoids) and the corrected anisotropy degree (Pj) as defined by Jelinek (1981). The orientation of the axes is analyzed for the geological interpretation of the strain, since it reflects the orientation-distribution of all minerals: diamagnetic, paramagnetic and ferromagnetic s.l. (Borradaile and Jackson, 2004). The magnetic foliation plane is perpendicular to the k_{min} axes, whereas the magnetic lineation is the orientation of k_{max} axes when certain degree of clustering is defined. The anisotropy data software Anisoft (Chadima et al., 2020), was used to obtain the scalar and directional magnetic fabric data.

In addition, selected samples from four sites were cooled down to 77 K (liquid nitrogen) to measure the low temperature AMS (LT-AMS). These measurements enhance the paramagnetic susceptibility and allow separating the magnetic signal of the AMS at room temperature from the paramagnetic signal. In a paramagnetic mineral, if magnetic interactions are neglected, the magnetic susceptibility follows the Curie-Weiss law: $Kp = C/(T - q)$; where Kp is the mass susceptibility which increases with decreasing temperature (T), for a paramagnetic mineral. C is a constant (Curie constant) and q is the paramagnetic Curie temperature. Plots of the inverse susceptibility (1/K) versus temperature give the q (Parés and van der Pluijm, 2014 and references therein). In a perfect paramagnetic material the magnetic susceptibility at low temperature will be 3.8 times higher than at room temperature (Parés and van der Pluijm, 2002a and references therein). The analyses of the AMS at low temperature are particularly useful in separating fabrics when the paramagnetic phyllosilicates are present (Parés and van der Pluijm, 2014) but this technique also gives good results in chalk rocks with less than 5 % of paramagnetic minerals (Issachar et al., 2016). In this work, we follow a similar procedure to cool down the samples by immersing them in liquid nitrogen as in Lüneburg et al. (1999).

Thermomagnetic curves were analyzed in selected samples: i) the temperature dependence of magnetic susceptibility was measured in 12 samples using the KLY3-CS (AGICO Inc.) at the University of Zaragoza and ii) the temperature dependence of the induced magnetization was measured in two samples using the variable field translation balance or Curie balance, (MMAVFTB, Petersen Instruments) at the Paleomagnetic Laboratory of the University of Burgos. Other rock magnetic analyses as the Isothermal Remanent acquisition curve (IRM), the coercivity of the remanence (back field) and hysteresis loops were measured using the same Curie balance (MMAVFTB, Petersen Instruments). The accompanying software Analyzer is used for visualization of results. All these analyses help to constrain the magnetic carriers present in the samples. These analyses are performed on powdered samples weighting 0.3–0.5 g.

The decay of the remanence during heating and after isothermal remanence magnetization at 1.9, 0.4 and 0.12 T along three perpendicular axes (Lowrie, 1990) were also performed at the University of Burgos in standard samples ~8 cm^3 in volume.

Thin sections of 11 samples were cut in two different directions, perpendicular and parallel to the magnetic lineation for optical microscope observations, using a LV 100 POL Nikon microscope (IGME Zaragoza – CSIC) and a KERN microscope and camera (ODC832) visualized through the MicroscopeVIS software (University of Zaragoza).

In order to obtain the content of calcium carbonate, calcimetries of 19 samples were performed using a Geoservices calcimeter (University of Zaragoza). The volume of CO_2 expelled by the sample (1 g powdered to 100 μm) after the reaction with 5 ml of HCl (5 M) in a closed 1 atm chamber is measured. The comparison with the CO_2 expelled by a standard sample gives the relative carbonate content of the sample.

4. Results

4.1. Rock magnetic analyses and calcimetries

In general, the heating curve differs greatly from the cooling run, i.e., they are not reversible, indicating transformation of the mineralogy during heating (Fig. 6). The paramagnetic behavior, which in the thermomagnetic curves of the temperature dependent magnetic susceptibility (KLY3-CS AGICO instrument) is shown by a hyperbolic decay at the beginning of the heating curve (from ~40 to 200 °C), appears only in five samples (LI-7, Fig. 6c; PO-4B, Fig. 6h; PO-2, Fig, 6i; PL-5, Fig. 6k; PL-1A, Fig. 6l). In all but one sample (SE-5, Fig. 6f) an increase of the magnetic susceptibility in the cooling curve occurs. This increase appears around the Curie temperature of magnetite (580 °C) (Collinson, 1983). The hyperbolic decay allows to calculate the ferromagnetic/paramagnetic behavior between 40 and 200 °C using Cureval 8.0 software (Chadima and Hrouda, 2009a). Values range from 67 % of ferromagnetic behavior in PO-4B to 8 % in PL-1A, PL-5 and LI-7.

In some samples (eight out of 12) the heating curve reveals the presence of a ferrimagnetic iron sulphide with an increase of the magnetic susceptibility from 240 °C - 270 °C onwards, reaching a peak (two samples show very clearly Hopkinson peaks, in LI-0 and SE-5, Fig. 6 a and f), with maximum values that occur at 264 °C in PL-1A to 318 °C in SE-5 (Fig. 6 l and f). These Curie temperatures (~325 °C) are typical of pyrrhotite 4C-type. Pyrrhotite 4C-type has a Curie temperature between 310 °C and 325 °C (Schwarz and Vaughan, 1972; Kontny et al., 2000, and references therein). This magnetic phase becomes cryptic or disappears after heating since it is seen as a small rise or not seen at all on the cooling curve. The magnetic susceptibility of the heating curve in the samples containing pyrrhotite decreases afterwards and increases again until the final decay, close to the Curie temperature of magnetite (~580 °C) (see Fig. 6). The cooling curve indicates the presence of magnetite, with a Curie temperature slightly higher than the one seen in the heating curve. Magnetite is generated during heating and it may have not been present before. The samples without pyrrhotite, show an increase of the magnetic susceptibility in the heating curve after 350–400 °C, with a final decay close to the Curie temperature of magnetite, indicating that a new magnetic phase was generated, except in LI-10, that shows a lower Curie temperature (Fig. 6d).

The thermal demagnetization of the remanence after applying the three-axes isothermal remanent magnetization (IRM) at 1.9, 0.4 and 0.12 T to a standard sample, shows a clear predominance of soft and intermediate coercivity minerals (the axes saturated at 0.12 T and/or at 0.4 T dominate the remanence) decaying at around 300 °C, which is typical of pyrrhotite (Lowrie, 1990), Fig. 6. The sample LI1-13 is an exception since magnetite is also present: a low coercivity mineral decaying at ~580 °C. In SE7 a mineral with strong coercivity is also present. It is probably hematite since the decay of the remanence appears at ~680 °C (Fig. 6m). The content of calcium carbonate is null in nine samples (out of 19), located in the Zinqueta valley and South of the

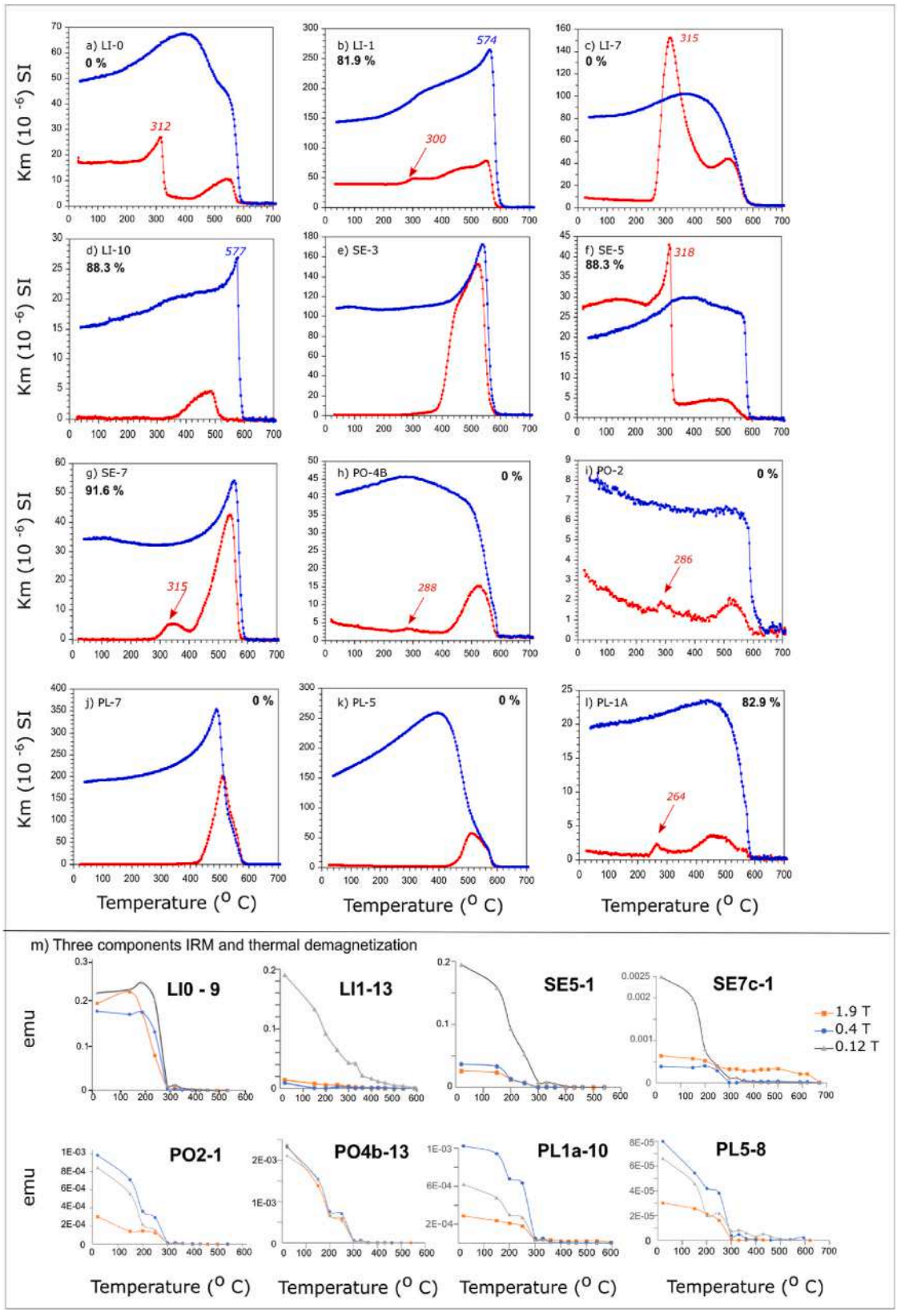

Fig. 6. a) to l) Temperature dependence of magnetic susceptibility. Red and blue curves are heating and cooling curves, respectively. Numbers are temperatures in ^{o}C, indicating with a red arrow the highest temperature on the rise of the magnetic susceptibility and in red without arrow the Curie temperature. Black numbers with percentage are $CaCO_3$ content obtained from calcimetries (see table in supplementary material for the results of the 19 samples). m) Decay of the remanence in each of the three axes during thermal demagnetization after applying at room temperature the three-component IRM. (For interpretation of the references to color in this figure legend, the reader is referred to the Web version of this article.)

Posets peak area plus two samples in the Llisat valley. In the Sen valley two samples show values lower than 40 % but the rest have values higher than 81 %. In five samples the presence of dolomite is suspected (S supplementary material).

The analyses in the Curie balance (MMAVFTB, Petersen Instruments) of the samples from the Llisat valley show the variability in the marbled limestones (LI-1) closest to the Millares granite with respect to the nearest site LI-0, where the latter shows stronger saturation magnetization (Ms) and coercivity of the remanence values (backfield, BF), which is compatible with the presence of an intermediate coercivity mineral such as an iron sulphide like pyrrhotite in LI-0 and a "soft" ferromagnetic mineral (low coercivity) such as magnetite in LI-1 (Collinson, 1983). The hysteresis loop of LI-0 with a clear wasp-waisted shape is probably related to the presence of different mineralogies or different grain sizes (Roberts et al., 1995). The presence of two magnetic phases can also be inferred from the thermomagnetic

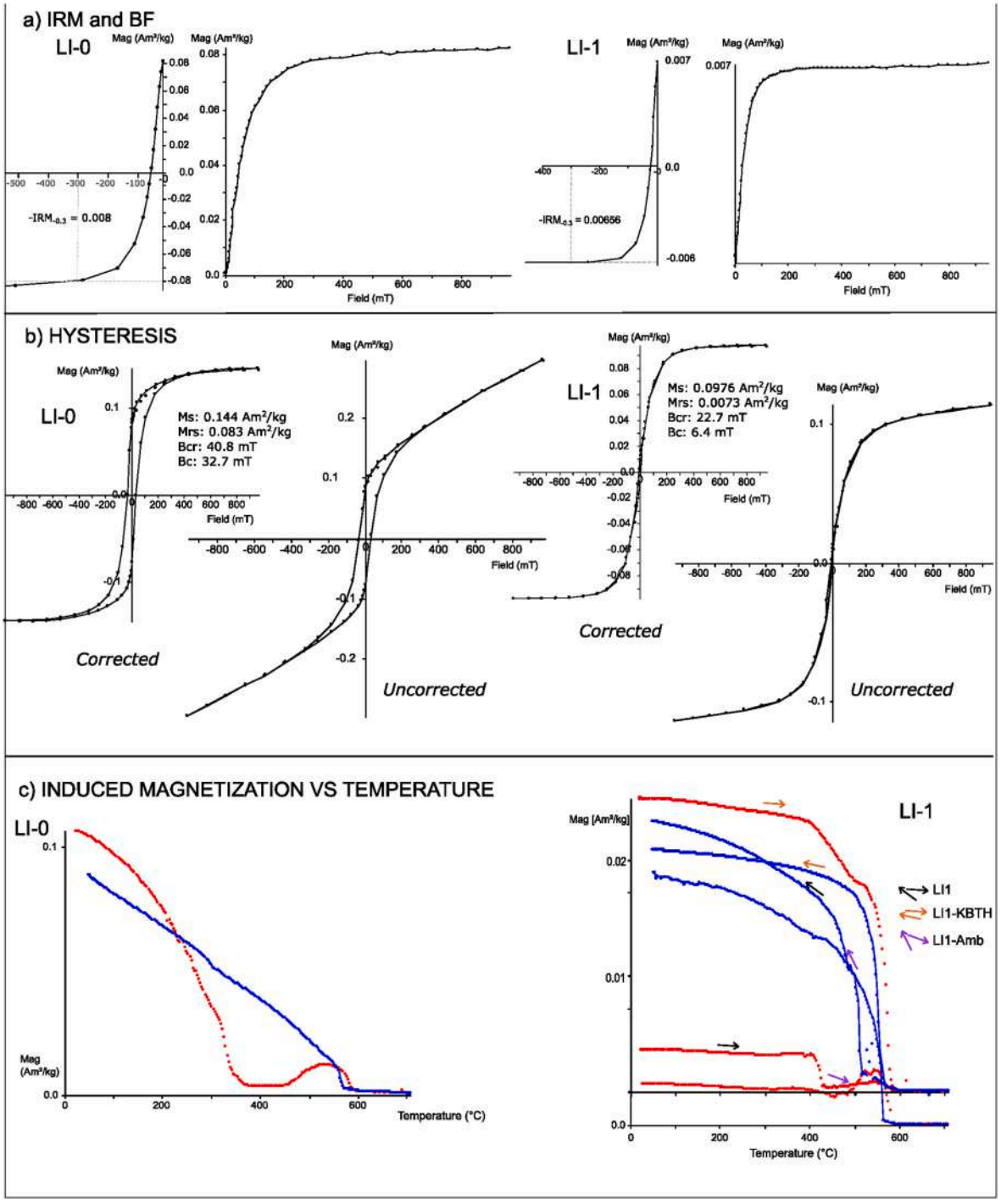

Fig. 7. Results of rock magnetism in the Curie balance. a) Acquisition of the Isothermal Remanent Magnetization (IRM) is on the right, and coercivity of the remanence (Back Field) on the left for each sample of sites LI-0 and LI-1. The value of IRM at −0.3 T is also shown (for subsequent use in the calculation of S-ratio). b) Hysteresis loops (corrected and uncorrected). c) Temperature dependent induced magnetization (heating path in red, cooling path in blue). For LI-1 several samples are presented; the colored arrows located on top of the curve refer to and are paired for the heating-cooling runs in the same sample. (For interpretation of the references to color in this figure legend, the reader is referred to the Web version of this article.)

curves (k – T, in Fig. 6 and induced magnetization-T, in Fig. 7c), with a larger induced magnetization, related to pyrrhotite, in LI-0 than in LI-1. Some variability within the marbled limestones of LI-1 appears in the induced magnetization/temperature curves, but in all samples the presence of pyrrhotite and magnetite seems plausible, from the observation of the two-step decay in the heating curves (red) at ~360 °C and ~580 °C, respectively using (Moskowitz (1981) method in the Analyzer software, Fig. 7c right).

4.2. Magnetic fabric

4.2.1. Values of the scalar parameters: km, T, pj

The averaged bulk magnetic susceptibility (Km) per site varies from 13700 E−6 SI in the marbled LI-1 site to −30.3 E−6 SI in LI-6 (Table 2) (see Table 1). Susceptibility values are below 500 E−6 (SI) for 30 out of the 35 sampled sites (Fig. 8a). The highest values are related to sites close to the granitic bodies where contact metamorphism is probably more intense due to hydrothermal fluids. The corrected anisotropy degree (Pj) shows very high values (>2) only in three sites: PL-7, SE-7(D) and LI-6 but these sites have Km close to zero. Therefore, the magnetic parameters of the ellipsoid are meaningless in terms of magnetic fabric (Hrouda, 2004). There are 11 sites in total with Pj averaged values higher than 1.4 (some of them with high standard deviations). Most of them come from the Devonian limestones of the Sen valley (enlargement of Fig. 8b, on the right), with slightly oblate magnetic susceptibility ellipsoids (T parameter between ~0.3 and ~0.1). In general, there is a predominance of oblate shapes (T parameter >0) with only two sites showing prolate shapes, PL-8 and PL-5 (1<T < 0). The average value of this parameter T varies between 0.878 (SE-3, Silurian) and −0.334 (PL-8, Devonian).

At low temperatures there is an increase of the magnetic susceptibility for SE-3 and PL-1, becoming closer to 3.8 times (3.3 and 3.6 respectively) the magnetic susceptibility at room temperature, indicating the predominance of paramagnetic minerals. Conversely, in LI-0 and LI-1 there is a very low, 1.2 and 1.1 respectively, increase of susceptibility, indicating that ferromagnetic carriers of the magnetic susceptibility ellipsoid (AMS) predominate (Fig. 9a–c). The shape parameter slightly increases at low temperature except for SE-3, where the average value changes from 0.901 (at RT) to 0.757 (at LT). However, the corrected anisotropy degree increases at low temperatures in LI-0, LI-1 and SE-3 (Fig. 9d and e). In paramagnetic carriers, particularly in sheet iron-silicates, an increase of k_{max} axes values has been described

Table 1
Location of samples. Name, coordinates (geographic coordinates, WGS84 datum), bedding plane (So) with orientation expressed according to the Right Hand Rule (RHR), cleavage plane (S1). Age according to the geological map, lithology and name of Formation. Grey background for sites with more than one hand sample.

Sector	SITE	Latitude (N)	Longitude (E)	So RHR (overturned when dip>90°)	S1 RHR	Age	Lithology/Fm
Llisat valley	**LI0**	42.6060	0.40511	050, 118	230, 54	Devonian	Slate/Castanesa
	LI1	42.60792	0.40482	065, 140	245, 40	Devonian	Marbled limestone
	LI2	42.60416	0.40435	300, 20	–	Devonian	Limestone/Fonchanina
	LI3	42.60067	0.40725	090, 158	–	Devonian	Limestone/Castanesa
	LI4 (A + B)	42.647805	0.50688	002, 23	–	Devonian	Grey limestone/ Fonchanina
	LI5 (A + B)	42.59486	0.40585	020,36	260,44	Devonian	Grey limestone/Castanesa
	LI6	42.59343	0.40708	196, 155	349, 20	Devonian	Limestone/Castanesa
	LI7r	42.59121	0.40897	230, 20	323, 24	Devonian	Limestone/Rueda
	LI8 (A + B)	42.5868	0.40883	080, 135	250, 37	Devonian	Silt/Manyanet
	LI9r	42.58059	0.40819	150,05		Devonian	Limestone/Castanesa
	LI10	42.59379	0.40747	114, 140	300, 38	Devonian	Limestone/Castanesa
Sen valley	**SE1**	42.60733	0.37226	285, 35	265, 50	Devonian	Limestone/Rueda
	SE2	42.60796	0.37351	215, 29	173, 36	Devonian	Limestone/Castanesa
	SE3	42.60653	0.37092	290, 22	300, 22	Silurian	Black shales/slates
	SE4 (A + B)	42.61645	0.38621	164, 140	313, 34	Devonian	Limestone/Castanesa
	SE5	42.61645	0.38621	346, 25	336, 35	Devonian	Limestone/Castanesa
	SE6 (A + B)	42.61369	0.38196	094, 160	287, 18	Devonian	Limestone/Castanesa
	SE6C	42.61369	0.38196	274, 10	287, 18	Devonian	Limestone/Castanesa
	SE7C-hinge	42.60847	0.37376	280, 05	237, 25	Devonian	Limestone/Castanesa
	SE7 (A + B + D)	42.60847	0.37376	118, 153	323, 37	Devonian	Limestone/Castanesa
Zinqueta valley	**PL1A**	42.67783	0.40165	330.17	100, 65	Devonian	Shaly limestone/Rueda
	PL2A	42.6780	0.40576	200,50	102.62	Devonian	Shaly limestone/Rueda
	PL3 (A + B)	42.67586	0.540496	274, 100	075,40	Devonian	Grey limestone/Rueda
	PL4	42.66945	0.39981	355,65	355,65	Ordovician-Silurian	Shale
	PL5	42.66186	0.3884	010,30	258, 58	Ordovician-Silurian	Silt
Near Posets peak	**PL6 (A + B)**	42.6417	0.41246	277, 42	–	Devonian	Slate/Rueda-Castanesa
	PL7	42.6492	0.40841	291, 36	291, 36	Devonian	Limestone/Rueda-Castanesa
	PL8	42.64051	0.41571	013,58	230,81	Devonian	Limestone/Rueda-Castanesa
	PL9 (A + B)	42.64051	0.41571	290, 59	280, 88/334, 68	Devonian	Limestone/Rueda-Castanesa
	PO1	42.63624	0.44384	022, 62	330, 85	Devonian	Limestone/Rueda-Castanesa
	PO2	42.63624	0.44384	025, 75	330, 85	Devonian	Limestone/Rueda-Castanesa
	PO3	42.63624	0.44384	347, 81	332, 75	Devonian	Limestone/Rueda-Castanesa
	PO4B	42.63602	0.44357	060, 85	332, 75	Devonian	Limestone/Rueda-Castanesa
	PO4 (A + C)	42.63602	0.44357	006, 80	060, 85/ 332,75	Devonian	Limestone/Rueda-Castanesa

Table 2
Averaged values of Km, Pj, T and their standard deviation. n/N: number of considered samples/number of analyzed samples. Grey background for sites with more than one hand sample. Numbers in red in sites where parameters have no meaning in terms of magnetic fabrics and sites with confidence angles higher than 25° for k_{max} and k_{min} axes. Name and stratigraphic unit (or age) of the sites. Orientation of the three axes of the magnetic susceptibility ellipsoid (Dec/Inc: Declination/Inclination) and confidence angles in geographic coordinates. R is for Rueda Fm, Cast. and C are for Castanesa Fm, Fon. for Fonchanina Fm, Many for Manyanet Fm.

SITE	n/N	Km (SI) E−6		Pj		T		Fm *(or age)*	k_{max}		k_{int}		k_{min}	
		Aver.	St. Dev.	Aver.	St. Dev.	Aver.	St. Dev.		Dec/Inc	Conf. Angles	Dec/Inc	Conf. Angles	Dec/Inc	Conf. Angles
LI0	12/12	1950	349	1.533	0.045	0.109	0.081	Castanesa	49.3/9	2/1.6	140.5/7.2	2.2/1.6	268.3/78.4	2.3/1.8
LI1	18/18	13,730	7960	1.301	0.091	0.344	0.358	Castanesa	359/30	45.2/7	92/5	45.1/11.8	191/60	12.6/7.6
LI2	16/16	270	49.1	1.222	0.034	0.795	0.073	Fonchanina	55.3/6.4	15.2/3.9	325/2.3	15.2/2.6	215.3/83.2	4.7/1.4
LI3	13/13	193	16.7	1.211	0.038	0.682	0.070	Castanesa	10/21.2	7.2/2.2	278.2/4.6	7.2/2.8	176.6/68.3	3.3/1.5
LI4 (A + B)	21/23	3.08	5.56	1.218	0.398	0.065	0.475	Fon.	42/14	15.1/3.5	139/24	15.1/3.8	285/62	4.2/3.1
LI5 (A + B)	30/31	59.2	74.5	1.061	0.057	0.184	0.370	Cast.	61.8/24.8	65.4/24.5	320.5/23	65.5/20.9	193.1/55	25.2/21.1
LI6	15/15	**−30.3**	2.2	**2.150**	**2.188**	−0.265	0.430	Castanesa	102.6/0.7	32.4/2.5	12.4/10.7	32.3/4.4	196.4/79.2	5.4/3.5
LI7r	12/12	279	28.4	1.300	0.005	0.829	0.026	Rueda	32/12	6.4/5	299/14	7.3/4.1	161/72	6.6/3.4
LI8 (A + B)	29/29	225	149	1.424	0.296	0.638	0.152	Many.	55.6/16.5	7.1/4.3	316.4/28.5	5.4/3.4	171.9/56.2	6.8/2.4
LI9r	14/14	18.8	3.03	1.008	0.003	0.015	0.339	Castanesa	100/76	29.7/17	199/2	33.3/15.8	289/14	23.6/17
LI10	12/12	12.2	2.71	1.297	0.023	0.886	0.038	Castanesa	22/30	14.7/1.3	289/7	14.7/1.1	187/59	1.5/1.1
LI10B-hinge	15/15	**0.28**	1.41	**1.811**	**2.459**	0.092	0.524	Castanesa	14/16	18.8/8.5	284/1	18.6/7.6	191/74	12/3.5
SE1	16/17	39.5	25.8	1.276	0.139	0.485	0.316	Rueda	76.4/18.1	11.9/3.9	337.2/26.2	13.8/5.2	197/57.3	9.4/3
SE2	18/18	842	689	1.693	0.129	0.250	0.237	Castanesa	13.5/47.3	8.4/7.4	269.6/12.5	7.7/6.2	168.9/40	8.3/6.4
SE3	17/17	60.4	8.66	1.091	0.019	0.878	0.047	*Silurian*	47.6/21.1	16.1/2.3	312.5/13.1	16.1/2.2	192.8/64.8	2.8/2.1
SE4 (A + B)	30/30	77.7	91	1.192	0.144	0.084	0.379	Cast.	31/24	13.4/6.6	128/14	14.4/12.8	246/61	13.9/6.7
SE5	13/13	1890	755	1.723	0.148	0.149	0.125	Castanesa	56/17	4.6/3.6	325/3	4.3/3.8	226/73	4.3/3.8
SE6 (A + B)	29/29	71.8	43.9	1.776	0.336	0.095	0.167	Cast.	305/4	9.6/3.6	36/19	6.4/3.7	203/71	9.6/5.2
SE6C	16/16	108	102	1.647	0.412	0.209	0.331	Cast.	93/1	6.1/4.1	3/4	6.7/4.5	197/86	5.8/4.7
SE7C-hinge	10/10	16.4	15.7	1.573	0.507	0.309	0.244	Cast.	34/1	23/7.5	304/7	25.6/13.1	133/82	21.8/5.8
SE7 (A + B + D)	49/49	45	65	2.450	1.484	0.222	0.481	Cast.	45/1	35.1/4.8	315/18	35.2/11.7	137/72	12.9/4.5
PL1A	10/10	47	5.31	1.029	0.009	0.669	0.139	Rueda	82.7/79.4	36.6/2.7	277.5/10.3	36.9/3.5	187/2.7	8.3/2.3
PL2A	15/15	59.1	6.06	1.101	0.012	0.596	0.094	Rueda	139.6/52.5	10.8/3.4	277.6/29.7	10.9/3.8	20/20.7	4.6/2.7
PL3 (A + B)	29/29	227	46.5	1.175	0.032	0.497	0.205	Rueda	99.7/9.9	3.9/2.7	201.4/49.4	4.5/2.9	1.7/38.9	4.3/3.5
PL4	16/16	39.9	9.27	1.161	0.019	0.321	0.038	*Silurian*	56.3/42.7	1.6/1.3	288.4/33.7	2.7/1.3	176.8/28.8	2.7/1.5
PL5	17/17	183	27.9	1.103	0.005	−0.196	0.117	*Silurian*	79.3/20.4	2/1.3	344.6/12.2	3.3/1.6	225.7/65.7	3.2/1.1
PL6 (A + B)	25/27	125	96.9	1.230	0.151	0.284	0.151	R or C	360/51	6.3/2	129/28	18.2/3.4	234/26	18.3/4.6
PL7	15/15	**7.07**	4.09	**3.535**	**3.563**	0.581	0.427	R or C	61/32	7/2.9	315/24	6.9/3.7	1895/49	4.9/1.6
PL8	14/14	445	151	1.096	0.068	−0.334	0.219	R or C	69/46	6.7/3.8	327/11	7.2/5.8	227/42	6.8/4.6
PL9 (A + B)	20/22	901	835	1.300	0.129	0.105	0.085	R or C	55/29	5.2/2.9	322/4	5.2/4.7	225/61	4.8/2.9
PO1	11/11	247	45.2	1.136	0.022	0.665	0.102	R or C	117/46	12.5/2.5	210/3	12.5/4	302/44	4.6/1.6
PO2	6/6	218	15.1	1.119	0.004	0.330	0.090	R or C	100/62	2.2/1.2	359/6	3.2/1.4	266/27	3.3/1.4
PO3	13/13	247	67.1	1.081	0.028	0.577	0.148	R or C	25/74	5.5/2.5	158/11	5.1/3.8	250/11	4.4/3.4
PO4B	16/16	191	20.6	1.008	0.007	0.144	0.410	R or C	117/64	9,8/4	335/21	9.8/6.1	239/15	7.1/2
PO4 (A + C)	13/13	167	22.3	1.010	0.012	0.255	0.419	R or C	36/80	19/13.7	161/6	51/15	252/8	51/17.5

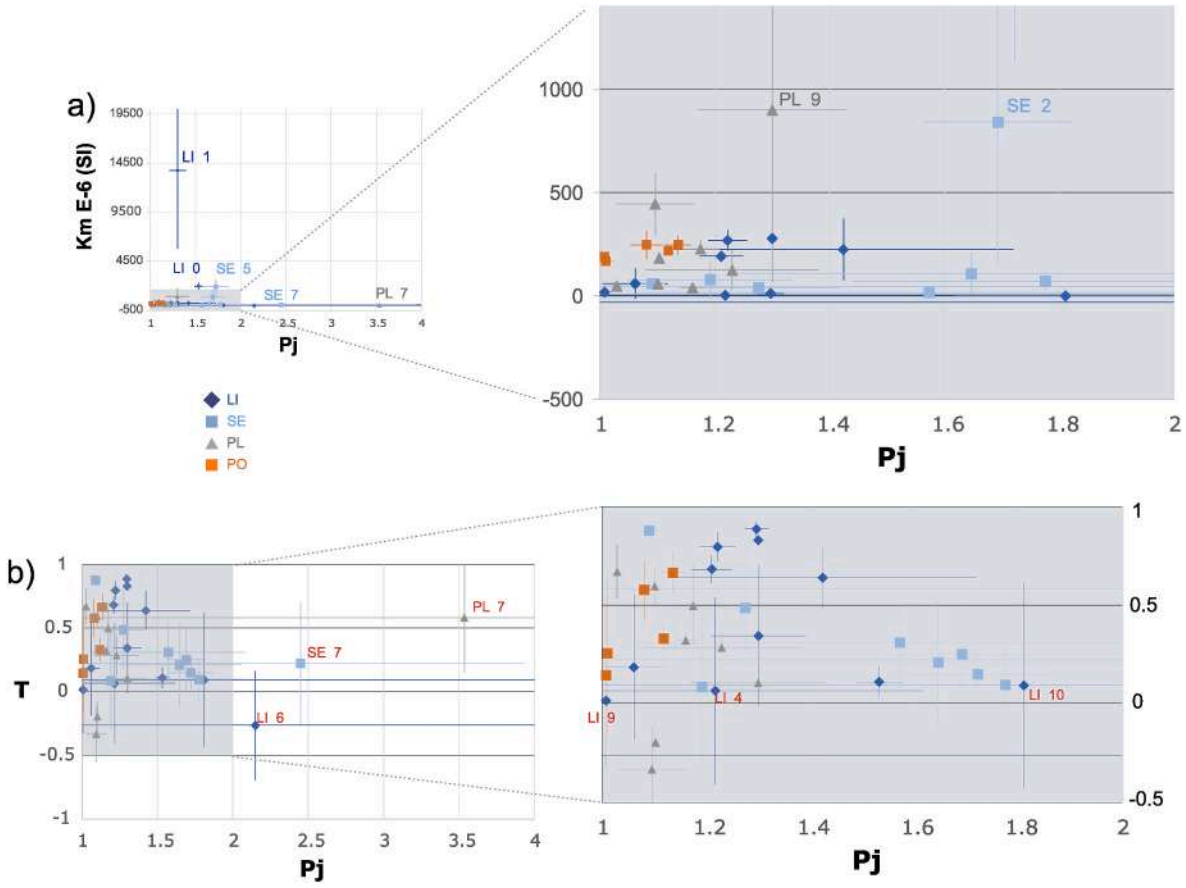

Fig. 8. Graphic representation of averaged values at every site and standard deviation of a) Km and Pj and b) T and Pj. Numbers in red correspond to sites where parameters are meaningless. (For interpretation of the references to color in this figure legend, the reader is referred to the Web version of this article.)

(Parés and van der Pluijm, 2002a), what explains the increase in Pj for SE-3.

4.2.2. Orientation of the magnetic susceptibility ellipsoid (AMS)

The magnetic lineation (clustering of k_{max} axes) is well defined in all but six sites (four in the Llisat valley, one in Sen valley and one in the Zinqueta valley). These sites are marked in Table 2 in red with their confidence angles when they are higher than 25°. In the Llisat and Sen valleys the sites with scattered k_{max} axes occur in the Castanesa Fm, and in the Zinqueta valley, in the Rueda Fm.

In the Llisat valley, bedding planes have low dips (≤~40°) in both normal and overturned limbs. The tectonic foliation development associated to folding (axial planar cleavage) provides an intersection lineation (L1) maximum at 30, 020 (plunge and azimuth). The magnetic lineation considering all samples provides a maximum at 14, 046 (plunge and azimuth) in geographic coordinates.

The magnetic lineation lies on the cleavage plane and close to the intersection lineation (Fig. 10). There are sites where the cleavage plane is at very low angle to the bedding plane (LI-1, LI-10); in other sites (LI-2, LI-3, LI-4) it is not possible to distinguish between them. Sites LI-6 and LI-9 show different orientation of the magnetic susceptibility ellipsoid axes: in LI-6 the k_{int} axes are closer to the intersection lineation, whereas in LI-9 it is the k_{max} axis the one perpendicular to bedding/cleavage planes and the k_{min} axes are closer to the intersection lineation, although the axes of the site are strongly scattered; this would be a composite inverse fabric (k_{max} and k_{min} axes are interchanged). This site LI-9 also shows large quantities of calcium carbonate in the calcimetries (almost 95 %), probably has low content of paramagnetic phase, and the ferromagnetic minerals provide a scattered fabric. Another site with large quantities of calcium carbonate is LI-10 (clustered axes). Therefore sites LI1, LI5, LI6 and LI9 show scattered magnetic axis, as indicated by the large confidence angles (see k_{max} axes, for example), marked in red in Table 2 (above 25°). Some of these sites, such as LI6, LI9 and LI10 show very high calcium carbonate content in the calcimetries (LI5 is not analyzed), which corresponds with very low average values of the Km (except LI1). At low temperature there is no change in the orientation of the axes for LI-0 but the opposite occurs in LI-1, where the k_{min} axes at low temperature are roughly switched with the k_{max} axes at room temperature (Fig. 10). These sites have very low content of paramagnetic minerals and the magnetic susceptibility barely increases at low temperature (Fig. 9).

In the Sen valley, the magnetic lineation (11, 049) and the magnetic foliation are similar to those obtained in the Llisat valley. The magnetic lineation fits better with the intersection lineation between bedding and cleavage planes in SE-1, SE-4, SE-5 and SE-6 although the orientation of the k_{int} axes in SE-6 (38, 026) is closer to the intersection lineation for all sites (Fig. 11) (composite intermediate fabric). SE-7 shows a magnetic fabric neither related with bedding nor with cleavage planes whereas the k_{int} axes of SE-2 are closer to the intersection lineation of the site. At low temperature, the magnetic axes overlap with the ones at room temperature (SE-3) in the Silurian rocks and are better clustered, Fig. 11.

The content of calcium carbonate is high in some sites (i.e., SE05 has–88 %, and also in SE-1 and SE-7, Supplementary material). SE-5 and SE-7 show scattered axes in the AMS. However, as seen before, in SE-3 and LI-0 sites, the low temperature analyses of the AMS indicates a better clustering of the axes at low temperature, suggesting that paramagnetic minerals develop a more grouped AMS ellipsoid than the whole rock, that is, ferromagnetic minerals would be more scattered, eventhough the paramagnetic content in LI-0 is very low.

In the Zinqueta valley and in sites near the Posets peak, folds show

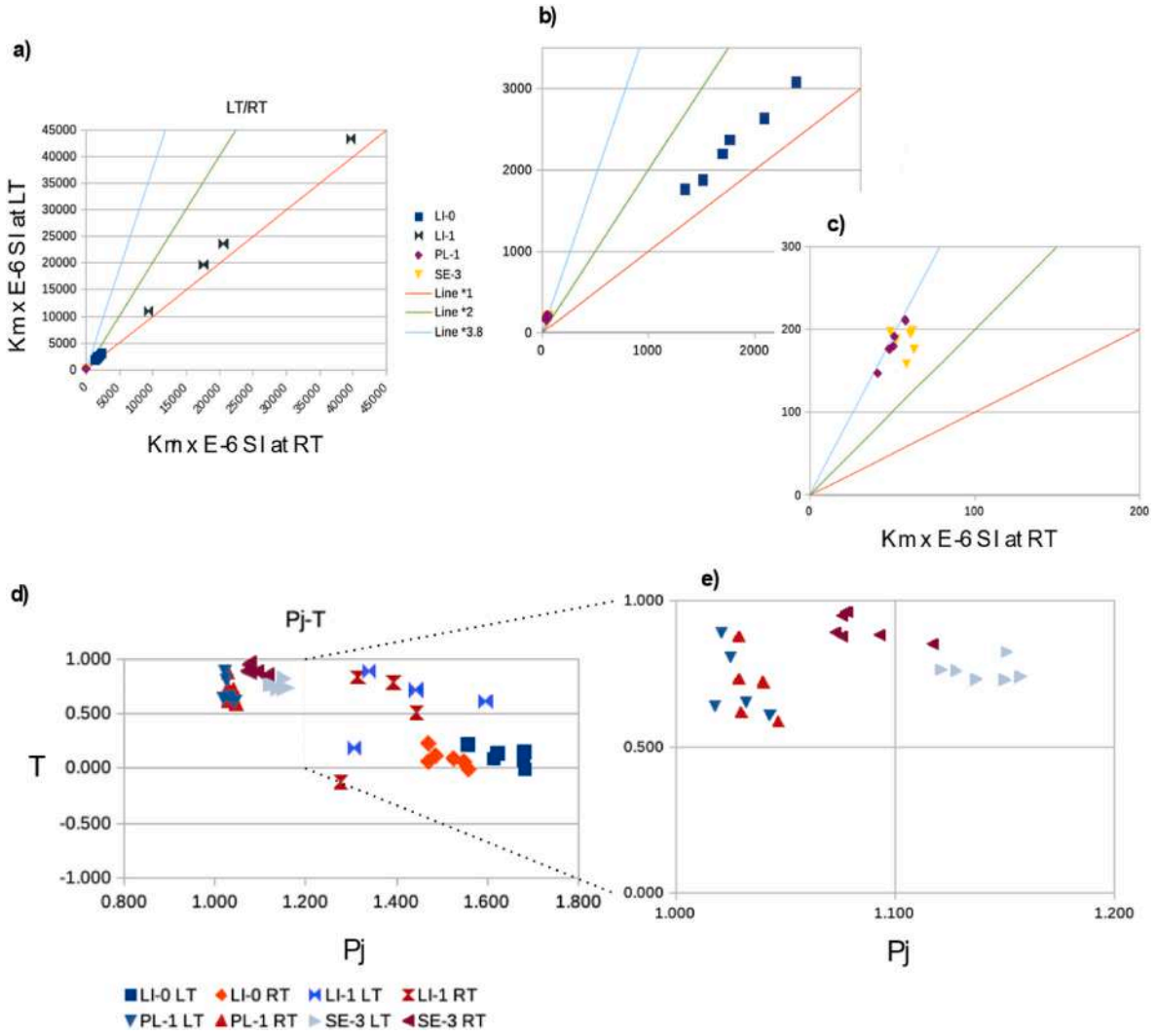

Fig. 9. Values of the magnetic susceptibility at room (RT) and low(LT) temperature (a) and enlarged in (b) and (c). Values of Pj and T at room and low temperature in (d) and enlarged in (e). See table in the supplementary material.

steeper limbs (Figs. 12 and 13) and fold interference features. Cleavage planes in this area show a roughly constant orientation (E-W strike and southward dips). The magnetic lineation considering all samples provides a maximum at 10, 090 in geographic coordinates (Fig. 12b). In PL-1 and PL-2, the k_{int} axes are closer to the intersection lineations, but only in PL-2 the magnetic lineation lies on the cleavage plane at room temperature. At low temperature site PL-1 (the value of Km is closer to an increase of 3.8 times the value at room temperature, indicating high content of paramagnetic minerals), the magnetic lineation roughly clusters near the intersection lineation (composite normal magnetic fabric), whereas at room temperature the k_{int} axes cluster near the intersection lineation (composite intermediate magnetic fabric). In any case, the k_{min} axes are in the same position at low and room temperature, horizontal near the 180° in azimuth, closer to the pole to the tectonic foliation. PL-3 and PL-2 sites clearly show the k_{min} axes clustered at the pole of the tectonic foliation (Fig. 12).

In the Posets peak area there are three maxima of the magnetic lineation, all with a NE orientation in geographic coordinates, the absolute maximum with lower plunge, close to the horizontal. Interestingly, in PO-1,2,3 the magnetic lineation lies on the bedding plane, in a subvertical position in geographic coordinates, and close to the intersection lineation, as well as in PO-4. IN PO-4 some interchange of axes (mostly between k_{max} and k_{min} axes) occurs at room temperature. Furthermore, in PL-8, 9, the magnetic lineation overlaps the intersection lineation (Fig. 13). Cleavage in these sites (PL8-9) is axial planar to outcrop-scale folds but oblique to folds in PO-1. In PL-6 and PL-7, no cleavage was identified in the field and the magnetic lineation is here contained within the bedding planes, plunging moderately to the N-NE, is here contained within the bedding plane. The minimum axes are not clustered to the pole to the bedding (composite anomalous magnetic fabric).

4.3. *Thin sections*

The observations under the petrographic microscope (transmitted light) allow to determine that the main mineral components are calcite and phyllosilicates with opaque minerals as accessories (Fig. 14). Quartz is also present and all observed grains show undulose extinction in crossed polarizers. Large calcite crystals and andalusite are the main components in LI1 together with opaques. The typical appearance of the black shales of Silurian time of SE-3 is shown on the left of the thin section, with small grain size of calcite, phyllosilicates and opaques, but there are also large grains of calcite, as seen on the right of the thin section. In SE-6 calcite predominates with idiomorphic opaque grains.

In PL-2A large calcite crystals and quartz with undulose extinction appear. Preferred orientation of calcite crystals, phyllosilicates and opaque minerals consistent with bedding can be seen in SE-6, PO-1 and PO-3 with smaller grain sizes. Other preferred orientations (LI-8) can be

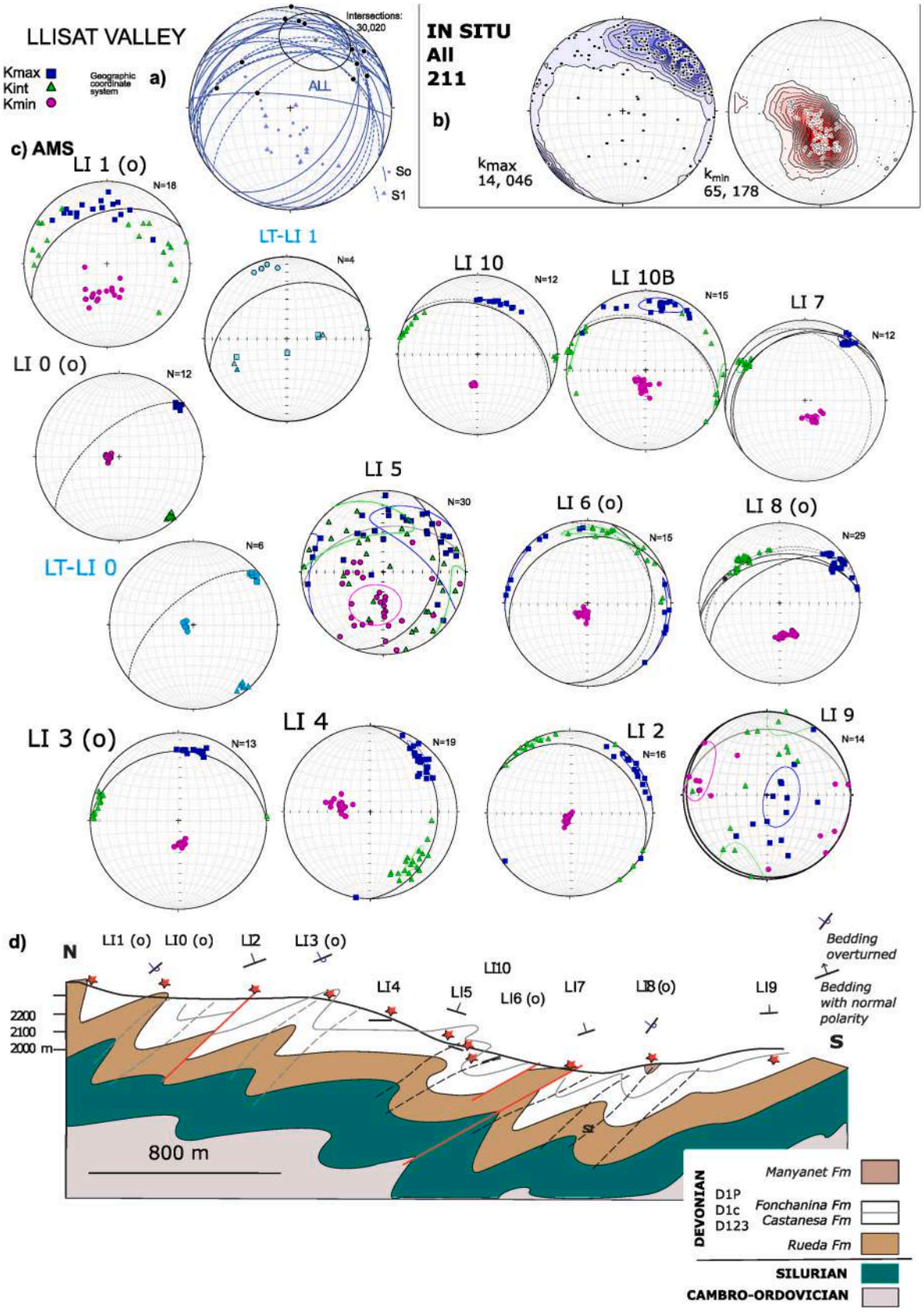

Fig. 10. Stereoplots of a) bedding and cleavage planes in the Llisat valley, b) density diagrams for the whole data set of the magnetic susceptibility ellipsoid axes (AMS) at room temperature; in blue: k_{max} axes, in red: k_{min} axes. c) AMS results in geographic coordinates (in situ) at room and low temperature (LT-LI 0 and LT-LI 1). d) Schematic cross-section of the location of the sampled sites. Symbols of AMS ellipsoids: squares: k_{max} axes, triangles: k_{int} axes, circles: k_{min} axes. (For interpretation of the references to color in this figure legend, the reader is referred to the Web version of this article.)

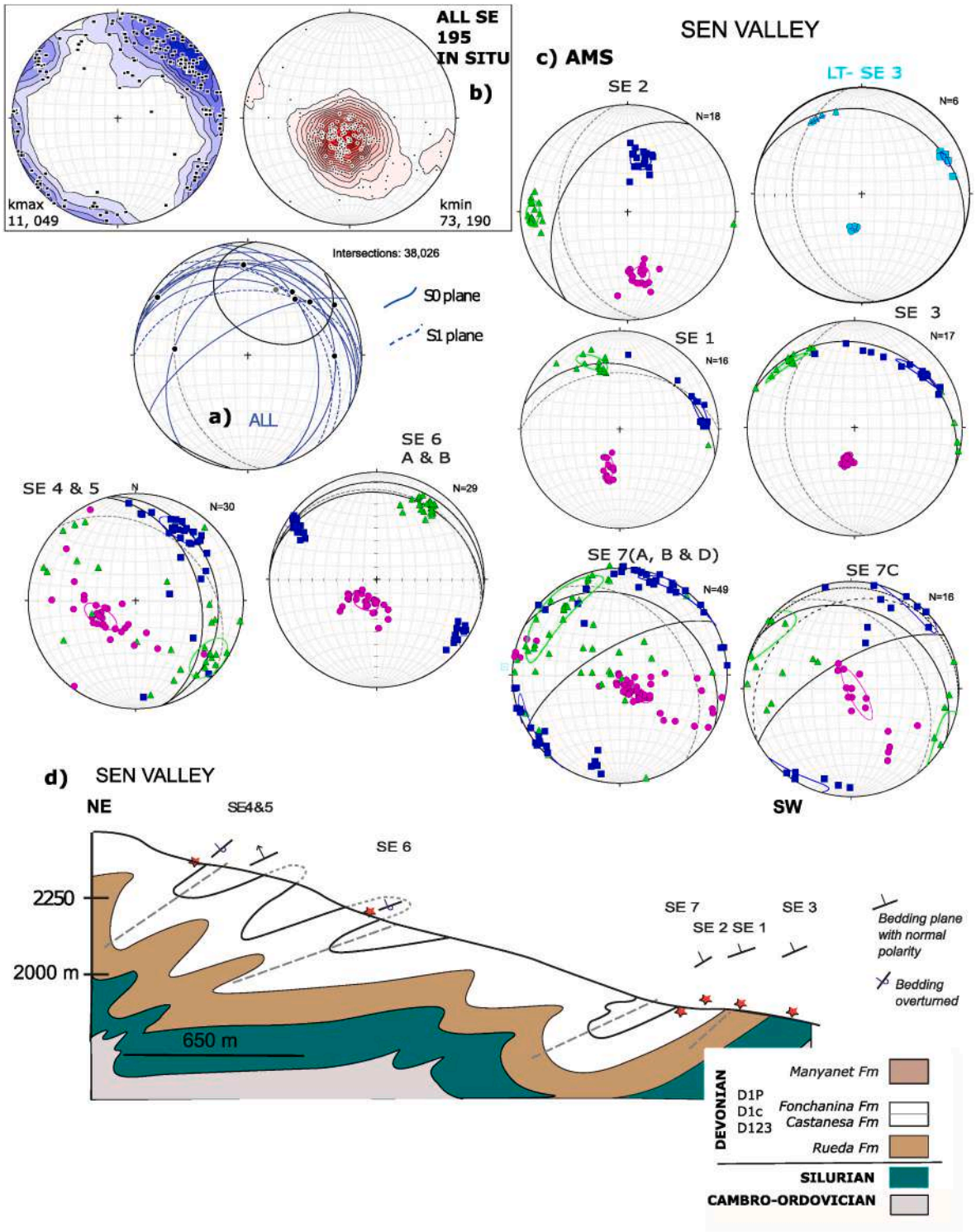

Fig. 11. Stereoplots of a) bedding and cleavage planes in the Sen valley, b) density diagrams for the whole data set of the magnetic susceptibility ellipsoid axes (AMS) at room temperature (in blue, k_{max} axes, in red, k_{min} axes). c) AMS results in geographic coordinates (in situ) at room and low temperature (LT-SE 3). d) Schematic cross-section of the location of the sampled sites. Symbols of AMS ellipsoids: squares: k_{max} axes, triangles: k_{int} axes, circles: k_{min} axes. (For interpretation of the references to color in this figure legend, the reader is referred to the Web version of this article.)

related to foliation or shear planes. In the sites nearest to the contact of the Millares granite, PL-5, PL-7 and LI-1 there are chiastolite crystals indicating contact metamorphism.

5. Discussion

5.1. Carriers of AMS

The combination of the analyses of the AMS performed at room and low temperature, and the classical rock magnetic analyses such as

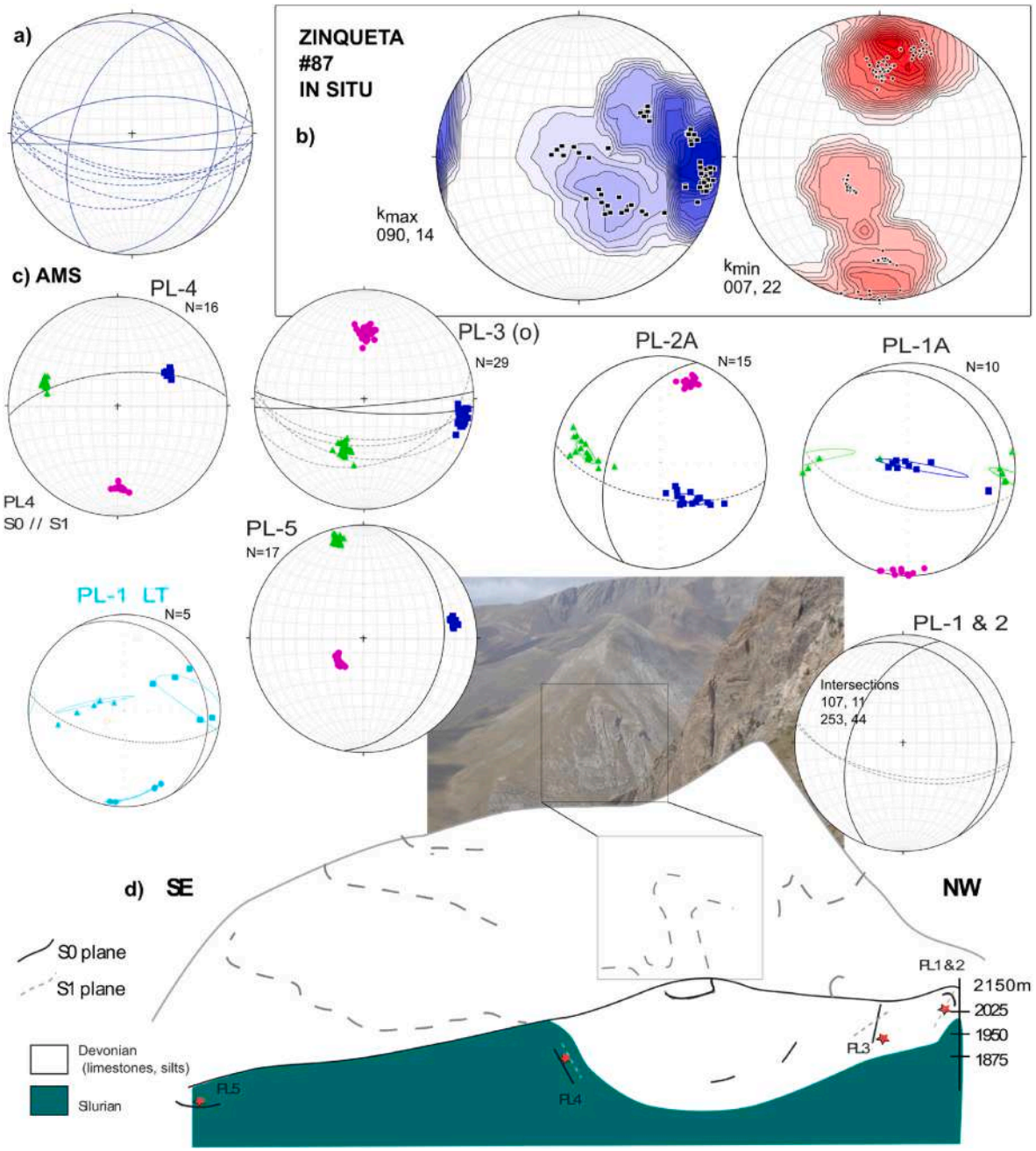

Fig. 12. Stereoplots of a) bedding and cleavage planes in the Zinqueta valley, b) density diagrams for the whole data set of the magnetic susceptibility ellipsoid axes (AMS) at room temperature, in blue, k_{max} axes, in red, k_{min} axes. c) AMS results in geographic coordinates (in situ) at room and low temperature (PL-1). d) Schematic cross-section representing the location of samples, with a field picture representing the background of the slope for scale. Symbols of AMS ellipsoids: squares: k_{max} axes, triangles: k_{int} axes, circles: k_{min} axes. (For interpretation of the references to color in this figure legend, the reader is referred to the Web version of this article.)

thermomagnetic curves, hysteresis loops, IRM and back field in selected samples suggest that ferromagnetic (*s.l.*) iron sulphides are an important component of the magnetic mineralogy of the samples (see Fig. 6 with k-T curves). This adds to the relatively high coercivity seen in the hysteresis loops of LI-0 (with respect to LI-1) and the induced magnetization decay at temperatures lower than 400 °C (Fig. 7). This is corroborated by the lack of increase of the Km values at low temperature in LI-0 and LI-1 (Fig. 10). In these samples, the orientation of the magnetic fabric (AMS) at low temperature coincides with AMS at room temperature in LI-0 and appears to be reverse in LI-1, where the k_{min} axes at LT are switched with the k_{max} axes at RT. Inverse fabrics were described at first as related to the presence of single domain magnetite and/or ferroan-carbonates (Rochette, 1988; Oliva-Urcia et al., 2024 and references therein). More recently, inverse fabric in dykes have been related to different emplacement phases under different tectonic directions and not to the presence of single domain magnetite grains (Raposo, 2017, 2020). Nonetheless, there are few samples where paramagnetic minerals (phyllosilicates) are the main carrier: PL-1, SE-3, PL-5 and LI-7 (calculations after the hyperbolic decay in the k-T curves). In site PL-1 there is an interchange of k_{max} - k_{int} axes from RT to LT AMS, but the k_{max} axes (magnetic lineation) at low temperature, tend to be closer to the intersection lineation measured in the area, at low temperature the fabric is "normal" (follows the structural features), whereas at room temperature is an "inverse" fabric (k_{max} and k_{int} are interchanged). In addition, the low Km values found in some sites can be related to the calcite content (calcite is diamagnetic with a negative Km).

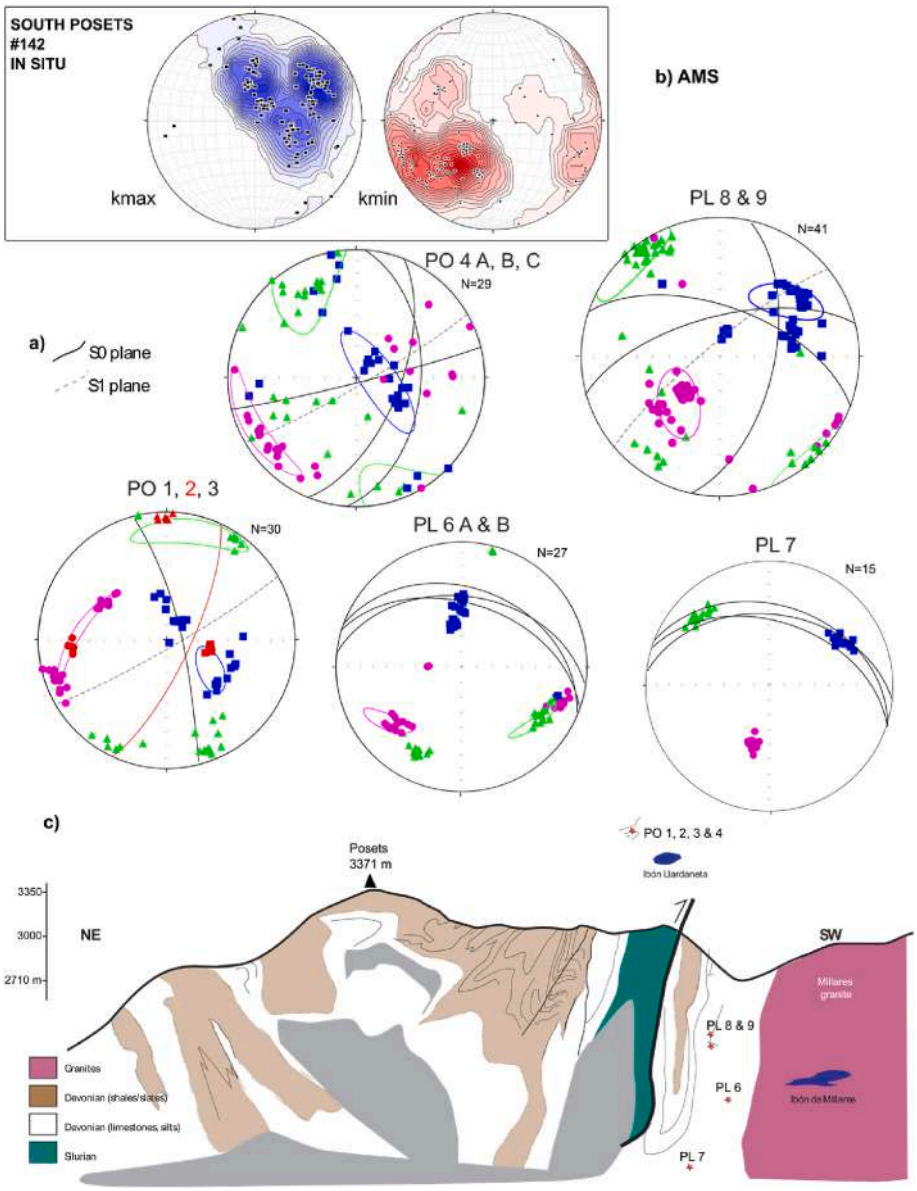

Fig. 13. Stereoplots of a) density diagrams for the whole data set of the magnetic susceptibility ellipsoid axes (AMS) at room temperature, in blue: k_{max} axes, in red: k_{min} axes. b) AMS results in geographic coordinates (in situ) at room temperature. c) Sketch of the location of the sampled sites (PO samples are located to the East of the sketch). Symbols of AMS ellipsoids: squares: k_{max} axes, triangles: k_{int} axes, circles: k_{min} axes. (For interpretation of the references to color in this figure legend, the reader is referred to the Web version of this article.)

Pyrrhotite is also present and has been also described as a remanence carrier in other Paleozoic rocks from the southern-central Pyrenean Axial Zone (Pastor-Galán et al., 2021) and northern Axial Zone (Izquierdo Llavall et al., 2020). In the southern-central Axial Zone, these rocks occupy structural positions which are analogous to the area sampled in this study. These authors suggest that the pyrrhotite-carried remanence is related to hydrothermal activity during the emplacement of the Late-Variscan granites. The emplacement of these granites has been determined to occur (Carreras and Druget, 2014), during Carboniferous times, about 300 Ma. Pastor-Galán et al. (2021) interpret the remagnetization carried by pyrrhotite as postfolding but pre-dating Alpine tilting and it shows equatorial inclinations which are in agreement with a Late Carboniferous age. These authors do not consider the possibility of neoformation of pyrrhotite in relation to burial, as proposed for clay-rich sedimentary basins (Aubourg et al., 2019). Other origins for iron-sulphides in basins are related to its neoformation in sulphidic and methanic sedimentary environments (Horng, 2018), since pyrrhotite is an iron sulphide solid solution that can have monoclinic structure (ferrimagnetic) or hexagonal structure (antiferromagnetic at room temperature). Recent investigations (Horng, 2018) suggest that magnetic properties can be used to distinguish authigenic sedimentary pyrrhotite in marine methane seepage environments from metamorphic pyrrhotite (and sedimentary greigite). One factor that allows distinguishing between authigenic and metamorphic pyrrhotite is the S-ratio (-$IRM_{-0.3}$/Mrs): when it is close to 1 (between 0.96 and 1) it can be attributed to a metamorphic origin, and lower values (between 0.52 and 0.78) can be considered as characteristic of sedimentary neoformed pyrrhotite (in nodules related to methane seepage, Horng, 2018). In our case, the available S-ratios for LI-0 and LI-1 are 0.96 and 0.89 respectively, closer to the metamorphic pyrrhotite values. Therefore, a secondary pyrrhotite is suggested to be present in this area too.

From the magnetic point of view, pyrrhotite is extremely anisotropic with magnetite-like low-field susceptibility values within the basal plane and values typical of antiferromagnetic material along the

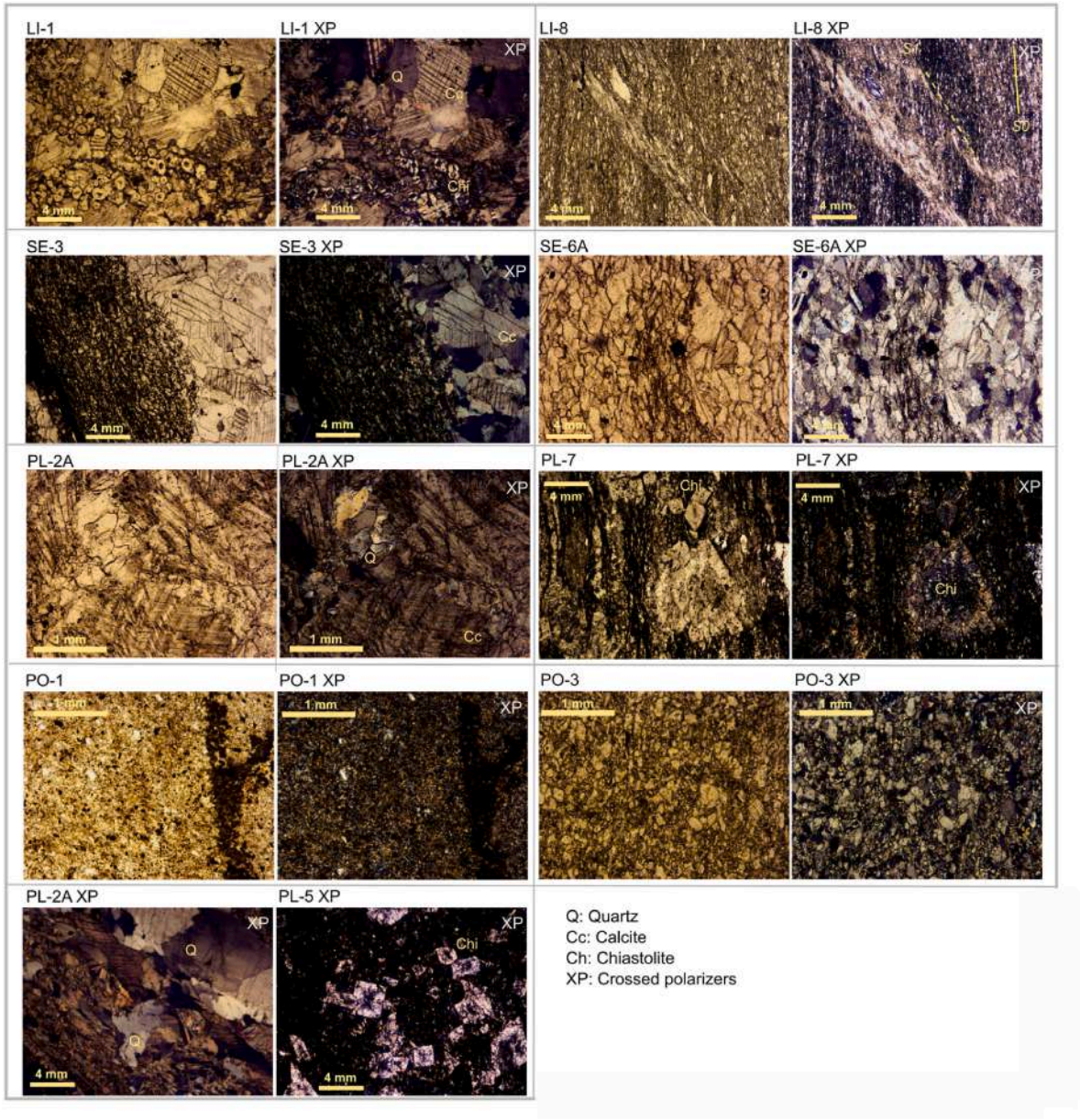

Fig. 14. Thin sections of selected samples showing the grain sizes, the petrofabric and the main composition of the analyzed rocks (chiastolite is a variety of andalusite).

crystallographic c-axis perpendicular to the basal plane. The low-field susceptibility of pyrrhotite is dependent on the grain size (low field susceptibility decreases with decreasing grain size; Dekkers, 1988), and the field strength and frequency utilized for its determination. Magnetic fabric orientation and anisotropy parameters also vary with field strength (Martín-Hernández et al., 2008 and references therein). In addition to pyrrhotite and phyllosilicates, magnetite is also present in the samples analyzed here as the "Lowrie test" and the thermomagnetic curves determine its presence.

The low temperature analyses of the magnetic fabric confirm the dominance of a ferrimagnetic carrier in LI-0 and LI-1 and paramagnetic carriers (phyllosilicates) in SE-3 and PL-1. The calculations from the hyperbolic decay of the k-T curves suggest that in PL-5 and LI-7 paramagnetic minerals dominate the sample, whereas in PO-3 ferromagnetic s.l. minerals predominate. The orientation of the magnetic susceptibility ellipsoid (AMS) is discussed in the next section in relation to the deformation endured by the Devonian (and Silurian) rocks, taking into account the information about the magnetic carrier. It is interesting to note that andalusite can behave as ferrimagnetic-like mineral when Ge and Fe interchange cations (Kakimoto et al., 2021). Andalusite (its variation chiastolite) are found in PO and PL-5, PL-7, LI-1 sites, near the Millares granite (Fig. 14).

5.2. Development of the magnetic fabric

The development of the composite magnetic fabric in these sedimentary rocks that have been subjected to at least two main deformation events (Variscan and Alpine orogenies) and with different content of ferrimagnetic and paramagnetic minerals is better understood for a region when sampling provides enough data and the data are taken together. As a first approximation, restoring bedding to the horizontal will indicate iwhether the magnetic susceptibility ellipsoid (AMS) is related to bedding (early deformational magnetic fabric) or to cleavage.

The Sen and Llistat valleys are less than 3 km apart and show recumbent kilometric folds (the same in the two valleys, or in equivalent positions) verging to the S-SE. The magnetic lineation defined by

ferromagnetic and paramagnetic grains coincides and in both areas this magnetic lineation is similar: 046,14 and 049,11 respectively. This shallowly-plunging, NE-SW magnetic lineation (in geographic coordinates) follows the elongation direction which overlaps with the intersection lineation between the bedding and foliation planes, which is commonly found in pelitic rocks (Parés and Van Der Pluijm, 2002b) and also related to the early stages of compression (layer parallel shortening), that is, the magnetic lineation is parallel to the strike of thrust and folds and therefore perpendicular to the shortening direction (García-Lasanta et al., 2014 and references therein).

In addition, after restoring bedding to the horizontal, the k_{min} axes are almost perpendicular to bedding (>65°) and the k_{max} axes are located within the bedding plane for ~70 % of the samples. The grouping of the magnetic axes indicates a tectonic origin, and following classical models about the evolution and development of the magnetic fabric, this type of fabric is described as a tectonic fabric and considered related to a tectonic event. Since the k_{max} axes are clustered on the bedding plane and the k_{min} axes are clustered perpendicular to the bedding plane, they can be related to an early tectonic phase (Parés et al., 1999, and Fig. 15) although in these isoclinal folds, the bedding and tectonic foliation show little difference between them.

The formation of folds in the Variscan orogen has been described, for the western part of the Axial Zone (near the Anayet basin, shown in Fig. 2), as a superposition of, firstly, large tight, west verging, kilometric scale ~ N340°E oriented recumbent folds, with axial planar cleavage, and secondly, asymmetric chevron folds with fold axis oriented 10, 080°. According to Rodríguez-Méndez et al. (2016), this second folding phase is related to the Alpine deformation and has been described as

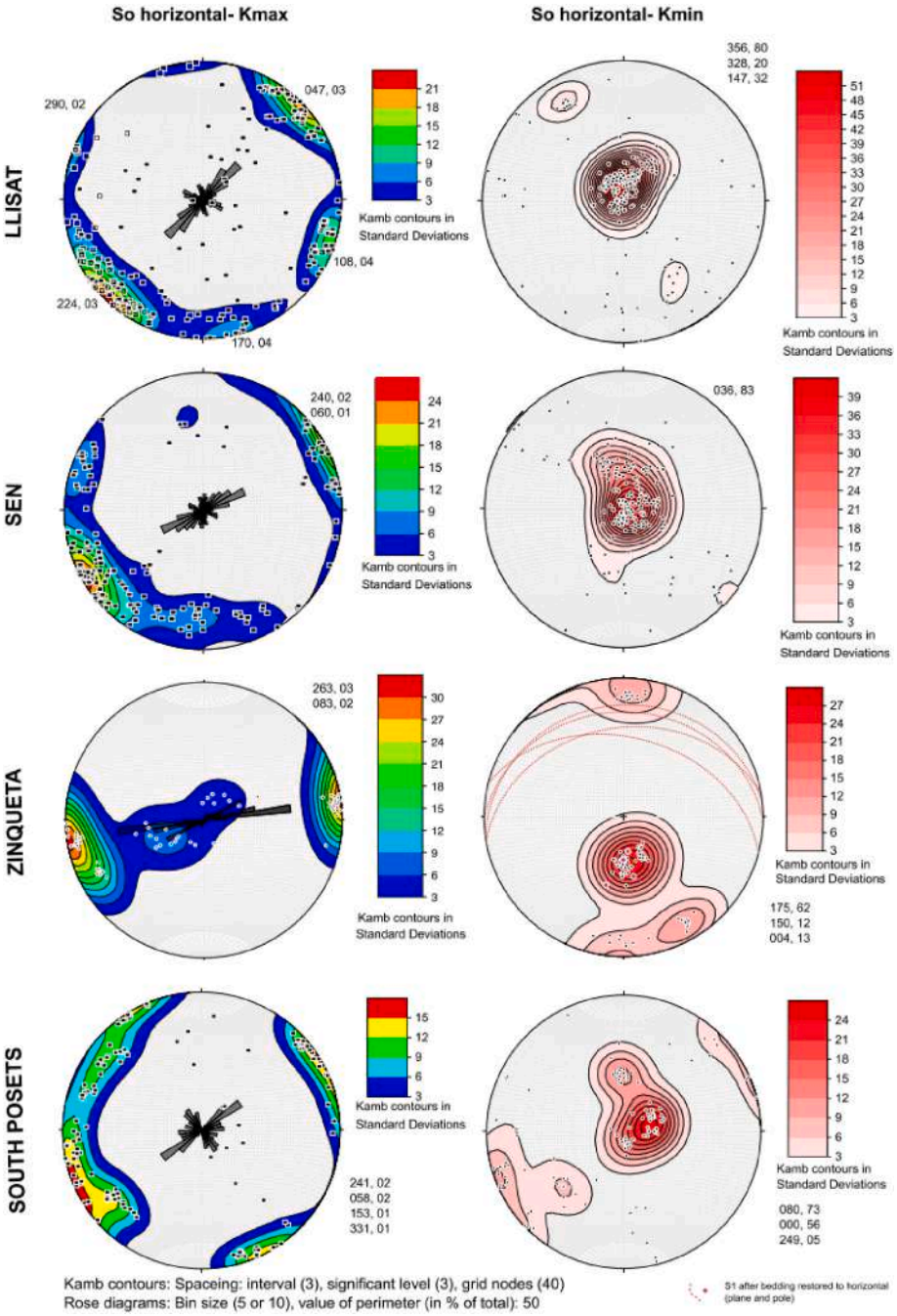

Fig. 15. Density stereoplots (lower hemisphere) of Kamb contours of k_{max} (left) and k_{min} (right) axes of the four areas after bedding correction. Rose diagrams of k_{max} axes are also plotted. Numbers indicate azimuth and inclination of the maxima obtained with the rose diagram.

creating a dispersion in the fold and cleavage trends. In addition, near the Posets area, the granite (~300 Ma) intrudes the Silurian-Devonian rocks with a sharp contact concordant with bedding and the dominant tectonic foliation (S2) (Esteban et al., 2021). This foliation is axial-planar cleavage associated with tight, isoclinal south-verging folds in the southern part (Sen and Llisat areas) and upright folds next to the northern pluton contact. These authors describe the deformation process leading to interference patterns of type 3 (Esteban et al., 2021).

Our structural data (bedding and tectonic foliation measurements) reflect a superposition in the Zinqueta valley and Posets area, where N-S fold axes postdate the E-W trending folds since the tectonic foliation is perpendicular to the N-S folding. In these areas a later modification of the magnetic fabric is clear since the minimum axes are not perpendicular to bedding. In the Zinqueta valley the magnetic fabric are related to the tectonic foliation, since a significant cluster of k_{min} axes locates around the pole to the tectonic foliation planes (Fig. 15).

Previous authors (Carreras and Druget, 2014, among others) described for the Axial Zone, two deformational phases during the Variscan orogeny, a first one (D1) that is related to a fold and thrust belt with localized, weak cleavage, and with low to very low degree of metamorphism and a second one (D2), that is related to a fold and thrust belt with cleavage development in a very shallow structural level. In D2 the metamorphism is restricted to aureolas around granitoids (in Esteban et al. (2021), they describe a 1 km of aureola of contact metamorphism around the Posets granite), which are late syn-tectonic plutons. Previous structural data and magnetic fabric studies of the Pyrenean granitoids have demonstrated that their emplacement was coeval with the main Variscan D2 transpressive event, and particularly, the Posets emplacement has been described as short-live event in the long D2 deformational phase (Esteban et al., 2021 and references therein). However, other studies based on structural data consider that pluton intrusion occurs after D2 (i.e., Maladeta granodiorite, to the east of the studied area) (García-Sansegundo, 1996; Poblet, 1991). Therefore, if in this area the Variscan D1 phase affects the rocks, the magnetic fabric developed during that Variscan D1 folding phase. The Variscan D2 events and subsequent alterations/neoformations related to the contact metamorphism during granite emplacement, apparently mimic the prior D1 fabric or have superimposed a new magnetic fabric. These upper-crustal metasediments, have been characterized by a South-verging folds (phase 2 b that rework an early tectonic foliation (schistosity in Denèle et al., 2014)) and a stretching lineation associated with a top-to the SW shear sense. Locally, phase 2 b folds show E-W trending cleavage (Denèle et al., 2014).

The sites of Llisat and Sen valleys are barely tilted by the Alpine thrust sheets, because they are located along the hangingwall flat of the Bielsa thrust (see Fig. 3a), which explains the close to horizontal elongation lineation found. Interestingly, the NE-SW orientation of the magnetic lineation (once bedding is restored to the horizontal) found in our study follows the regional bulk stretching lineation interpreted during the emplacement of the Millares granite through a dextral wrench regime (E-W shear) along a NW-SE fracture, syntectonic with the late stages of the Variscan Orogeny (Román-Berdiel et al., 2006). Either there is a parallelism between the strain associated to the recumbent folds (D1) and the emplacement of the granites (D2), or the D2 fabric superimpose and obliterates fabric D1. We have not observed the regional Alpine tectonic foliation which should be expected to be E-W-striking and North-dipping (Choukroune and Séguret, 1973; Izquierdo-Llavall et al., 2013 among others).

South of the Posets peak (North of the Millares granite) a similar orientation of the magnetic lineation is observed once bedding is restored to the horizontal (NE-SW) but another secondary directional maximum is also present, almost perpendicular to the first one (SSE-NNW). A tectonic plane close to the vertical is seen in this area except for PL-6 and PL-7, and the intersection lineation has a strong plunge. Therefore, the magnetic fabric can be interpreted to have a tectonic origin, with some degree of interchange between axes since there are samples from PO-4B and PO-4C sites that show their k_{int} axes perpendicular to bedding and k_{max} and k_{min} axes distributed within the bedding plane with strong scattering. This type of fabric probably developed during the Variscan D1 phase but some overlapping with other folding phases (Variscan D2 phase or Alpine deformation in relation to the ramp of Millares thrust, Fig. 3a) occurs. It is interpreted that any possible modification due to contact metamorphism or hydrothermal fluids during the emplacement of granite bodies (Posets and Millares granites) at ~300 Ma (age of Posets granite, Esteban et al., 2021) in D2 overlaps the "earliest deformation" fabric (D1) of most samples.

Finally, in the Zinqueta valley, the "earliest deformation" fabric is not clear, since the k_{min} axes do not overlap with the pole to the bedding plane although the k_{max} axes are located within it (Fig. 16). Particularly, there are two sites, PL1 and PL2, where the fabric can be considered as "tectonic" since the k_{max} axes are clustered on or near the tectonic foliation plane and the k_{min} axes are clustered at (or near) the pole to the bedding plane. Something similar occurs in site PL-3. This tectonic fabric represents an evolved stage of tectonic fabrics (Parés et al., 1999). In this area, folds are not recumbent but with an axial plane close to vertical, and a steeply south-dipping cleavage is found in most sites.

6. Conclusions

The magnetic study of ~600 standard samples of limestones, shales and slates distributed in four areas near the Posets and Millares massifs, in the Axial Zone of the Pyrenees, allows proposing their deformational evolution. The magnetic results provide criteria for differentiating two sectors: i) the Sen and Llisat areas, south of the Millares granite show an elongation direction related to the D1 Variscan folding phase, since the magnetic lineation follows the trend of fold axes and hence the intersection lineation. The magnetic fabrics corresponding to this orientation seem to have been enhanced during the D2 Variscan phase due to granite emplacement and the hydrothermal fluids and contact metamorphism that affects the mineralogical content. During this stage, pyrrhotite and chiastolite formed. The elongation direction obtained from the magnetic fabric fits with the emplacement model for the Millares granite from previous investigations. This second tectonic phase is responsible for fold interference in the other sectors, South Posets and Zinqueta valley. The South Posets area presents a steeply-plunging magnetic lineation in geographic coordinates.

The magnetic mineralogy of these rocks is complex, since magnetite, pyrrhotite, paramagnetic and diamagnetic minerals have been detected, but the predominant ferromagnetic and paramagnetic fabrics seems to mimic each other for most sites.

These new results suggest the co-existence of two different magnetic fabric developments: (i) overlapping of the secondary fabric (second tectonic phase) onto the first one (magnetic fabric are "early tectonic" since the k_{min} axes are perpendicular to bedding) (Llisat and Sen areas), and (ii) obliteration/modification of the first tectonic fabric (k_{min} axes perpendicular or oblique to the tectonic foliation plane) by the second tectonic phase (Zinqueta and Posets areas).

CRediT authorship contribution statement

B. Oliva-Urcia: Writing – review & editing, Writing – original draft, Visualization, Validation, Supervision, Resources, Project administration, Methodology, Investigation, Funding acquisition, Formal analysis, Data curation, Conceptualization. **T. Román-Berdiel:** Writing – review & editing, Validation, Supervision, Formal analysis. **P. Clariana:** Writing – review & editing, Methodology. **R. Soto:** Writing – review & editing, Methodology. **E. Izquierdo-Llavall:** Writing – review & editing, Methodology. **A. Casas-Sainz:** Writing – review & editing, Visualization, Data curation, Conceptualization.

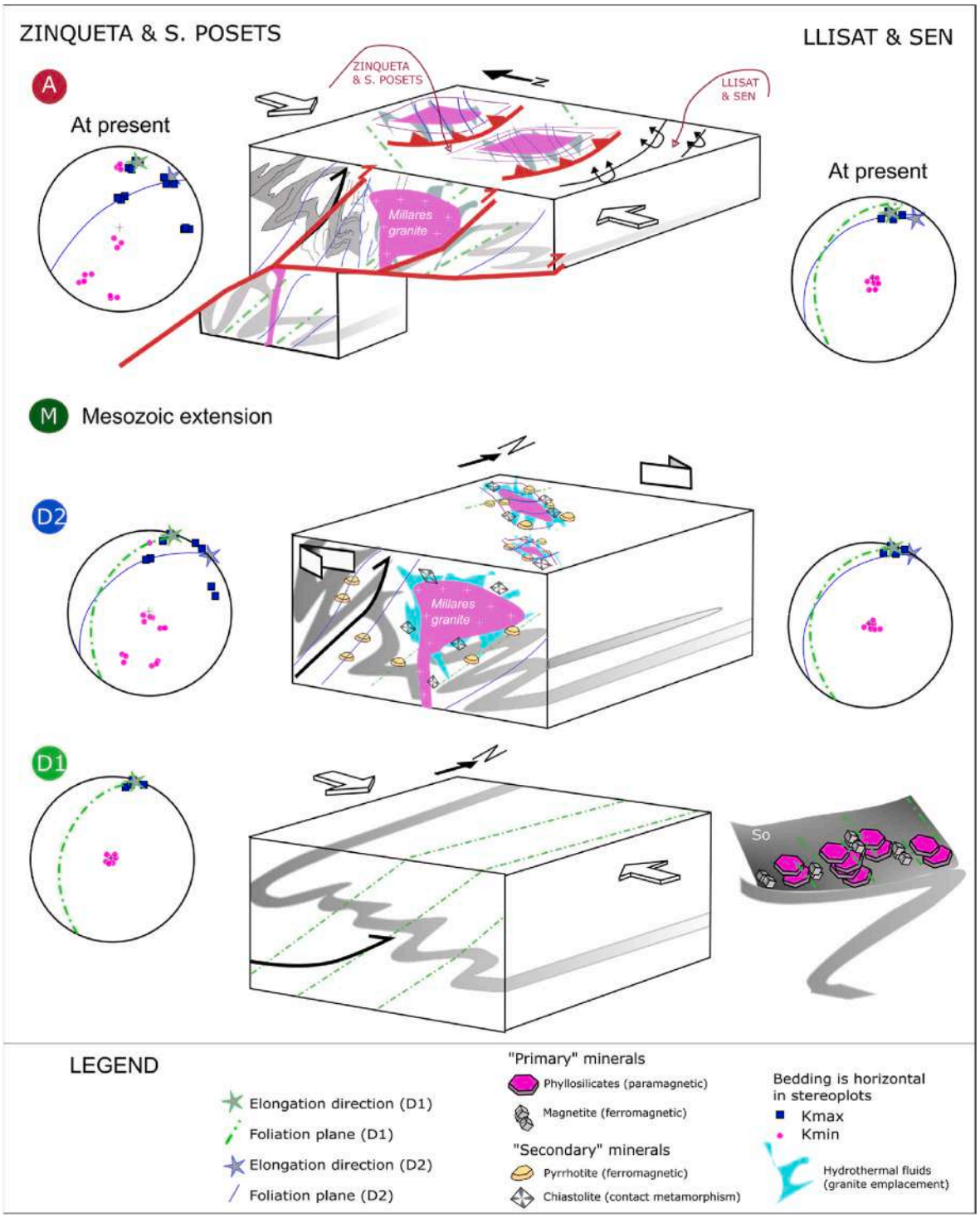

Fig. 16. Model of development of magnetic fabrics for two Variscan tectonic phases (D1 and D2) and theAlpine phase (A). Based on emplacement models of Denèle et al. (2014), Esteban et al. (2021), and Román-Berdiel et al. (2006). Superposition of D1 and D2 is interpreted, but the predominance of D2 phase can be also possible.

Declaration of competing interest

The authors declare that they have no known competing financial interests or personal relationships that could have appeared to influence the work reported in this paper.

Acknowledgements

Field work and thin section preparation was possible thanks to the "Ayuda a la Investigación de la Comarca de Sobrarbe" and National Project CGL 2017-90632-REDT. Authors would like to acknowledge the Servicio General de Apoyo a la Investigación-SAI (Servicio de Preparación de Rocas y Materiales duros and Servicio de Líquidos Criogénicos), Universidad de Zaragoza. Gustavo Higero Artigas is

acknowledged for doing the calcimetries. Project PID 2019-108753 GB-C22, funded by MICIN/AEI/10.3039/501100011033 and by "ERDF A way of making Europe" is also aknowledged. Proyecto del Gobierno de Aragón (E32_20R: Grupo de Investigación Geotransfer).

The Editor (I. Raposo) and three Reviewers are acknowledged for their insightful comments.

Appendix A. Supplementary data

Supplementary data to this article can be found online at https://doi.org/10.1016/j.jsg.2025.105495.

Data availability

Data will be made available on request.

References

Anastasio, D., Parés, J.M., Kodama, K.P., Troy, J., Pueyo, E.L., 2016. Anisotropy of Magnetic Susceptibility (AMS) Records Synsedimentary Deformation Kinematics at Pico Del Aguila Anticline. Pyrenees, Spain.

Aubourg, Ch, Jackson, M., Ducoux, M., Mansour, M., 2019. Magnetite-out and pyrrhotite-in temperatures in shales and slates. Terra Nova 31, 534–539.

Aubourg, C., Smith, B., Eshraghi, A., Lacombe, O., Authemayou, C., Amrouch, K., et al., 2010. New Magnetic Fabric Data and Their Comparison with Palaeostress Markers in the Western Fars Arc (Zagros, Iran) tectonic implications.

Averbuch, O., Frizon de Lamotte, D., Kissel, C., 1992. Magnetic fabric as a structural indicator of the deformation path within a fold-thrust structure: a test case from the corbières (NE Pyrenees, France). Journal of Structural Geology 14 (4), 461–474. https://doi.org/10.1016/0191-8141(92)90106-7.

Boiron, T., Aubourg, Ch, Grignard, P., Callot, J.P., 2020. The clay fabric of shales is a strain gauge. J. Struct. Geol. 138, 104130.

Borradaile, G.J., Jackson, M., 2004. Anisotropy of magnetic susceptibility (AMS): magnetic petrofabrics of deformed rocks. Geological Society, London, Special Publications 238 (1), 299–360.

Bouchez, J.L., 1997. Granite is never isotropic: an introduction to AMS studies of granitic rocks. In: Granite: from Segregation of Melt to Emplacement Fabrics. Springer Netherlands, Dordrecht, pp. 95–112.

Carreras, J., Capella, I., 1994. Tectonic levels in the Paleozoic basement of the Pyrenees: a review and a new interpretation. J. Struct. Geol. 16 (11), 1509–1524.

Carreras, J., Druget, E., 2014. Framing the Tectonic Regime of the NE Iberian Variscan Segment, 405. Geological Society, London, Special Publications, pp. 249–264.

Černý, J., Melichar, R., Všianský, D., Drahokoupil, J., 2020. Magnetic anisotropy of rocks: a new classification of inverse magnetic fabrics to help geological interpretations. J. Geophys. Res. Solid Earth 125 (11), e2020JB020426.

Chadima, M., Pruner, P., Šlechta, S., Grygar, T., Hirt, A.M., 2006. Magnetic fabric variations in Mesozoic Black shales, northern Siberia, Russia: possible paleomagnetic implications. Tectonophysics 418 (1–2), 145–162.

Chadima, M., Hrouda, F., 2009. Cureval 8 [Computer software].

Chadima, M., Hrouda, F., Jelinek, V., 2020. Anisoft 5. AGICO Inc [Computer software].

Choukroune, P., Séguret, M., 1973. *Carte Structurale Des Pyrénées, 1/500.000*. Université De Montpellier–ELF Aquitaine.

Collinson, D.W., 1983. Methods in Rock Magnetism and Palaeomagnetism: Techniques and Instrumentation. Springer Science & Business Media, 2013. Chapman and Hall.

De Sitter, L.U., Zwart, H.J., 1960. Tectonic development in supra and infra-structures of a Mountain chain. Proceedings 21st International Geological Congress 18, 248–256.

Debacker, T.N., Robion, P., Sintubin, M., 2004. The anisotropy of magnetic susceptibility (AMS) in low-grade, cleaved pelitic rocks: influence of cleavage/bedding angle and type and relative orientation of magnetic carriers. Geological Society, London, Special Publications 238 (1), 77–107. https://doi.org/10.1144/GSL.SP.2004.238.01.08.

Dekkers, M.J., 1988. Magnetic properties of natural pyrrhotite part I: behaviour of initial susceptibility and saturation-magnetization-related rock-magnetic parameters in a grain-size dependent framework. Phys. Earth Planet. Inter. 52, 376–393.

Denèle, Y., Laumonier, B., Paquette, J., Olivier, P., Gleizes, G., Berbery, P., 2014. Timing of granite emplacement, crustal flow and gneiss dome formation in the Variscan segment of the Pyrenees. Geological Society, London, Special Publications 405 (1), 265–287.

Esteban, J.J., Cuevas, J., Tubía, J.M., Hilario, A., Larionov, A., Sergeev, S., 2021. Posets pluton: a geochronological piece in the puzzle of the Axial Zone of the Pyrenees. Geol. Mag. 158 (12), 2264–2270.

Evans, M.A., Lewchuk, M.T., Elmore, R.D., 2003. Strain partitioning of deformation mechanisms in limestones: examining the relationship of strain and anisotropy of magnetic susceptibility (AMS). J. Struct. Geol. 25 (9), 1525–1549.

García-Lasanta, C., Oliva-Urcia, B., Casas-Sainz, A.M., Román-Berdiel, T., Izquierdo-Llavall, E., Soto, R., Calvín, P., Mussaid, B., El Ouardi, H., Kullberg, J.C., Villalaín, J. J., 2018. Inversion tectonics and magnetic fabrics in Mesozoic basins of the Western Tethys: a review. Tectonophysics 745, 1–23. https://doi.org/10.1016/j.tecto.2018.08.005.

García-Lasanta, C., Oliva-Urcia, B., Román-Berdiel, T., Casas, A.M., Hirt, A.M., 2014. Understanding the Mesozoic kinematic evolution in the Cameros Basin (Iberian Range, NE Spain) from magnetic subfabrics and mesostructures. J. Struct. Geol. 66, 84–101.

García-Sansegundo, J., 1992. Estratigrafía y estructura de la Zona Axial pirenaica en la transversal del Valle de Aran y de la Alta Ribagorça (Parte III). Bol. Geol. Min. 103 (1), 42–93.

García-Sansegundo, J., 1996. Hercynian structure of the Axial Zone of the Pyrenees: the Aran Valley cross-section (Spain-France). Journal of Structural Geology 18 (11), 1315–1325.

Gleizes, G., Leblanc, D., Bouchez, J.L., 1998. The main phase of the Hercynian orogeny in the Pyrenees is a dextral transpression. Geological Society, London, Special Publications 135 (1), 267–273.

Graham, J.W., 1966. Significance of magnetic anisotropy in Appalachian sedimentary rocks. The Earth Beneath the Continents, Geophys. Monograph Ser 10, 627–648.

Grasemann, B., Wiesmayr, G., Draganits, E., Fusseis, F., 2004. Classification of refold structures. J. Geol. 112 (1), 119–125.

Horng, C.S., 2018. Unusual magnetic properties of sedimentary pyrrhotite in methane seepage sediments: Comparison with metamorphic pyrrhotite and sedimentary greigite. J. Geophys. Res. Solid Earth 123 (6), 4601–4617.

Housen, B.A., Richter, C., van der Pluijm, B.A., 1993. Composite magnetic anisotropy fabrics: experiments, numerical models and implications for the quantification of rock fabrics. Tectonophysics 220 (1–4), 1–12.

Hrouda, F., 2004. Problems in interpreting AMS parameters in diamagnetic rocks. Geological Society, London, Special Publications 238 (1), 49–59.

Hrouda, F., Chadima, M., 2020. Examples of tectonic overprints of magnetic fabrics in rocks of the bohemian massif and Western Carpathians. Int. J. Earth Sci. 109 (4), 1321–1336.

Issachar, R., Levi, T., Lyakhovsky, V., Marco, S., Weinberger, R., 2016. Improving the method of low-temperature anisotropy of magnetic susceptibility (LT-AMS) measurements in air. G-cubed 17 (7), 2940–2950.

Izquierdo Llavall, E., Menant, A., Aubourg, C., Callot, J.P., Hoareau, G., Camps, P., Péré, E., Lahfid, A., 2020. Preorogenic folds and syn-orogenic basement tilts in an inverted hyperextended margin: the Northern Pyrenees case study. Tectonics 37 (7), e2019TC005719.

Izquierdo-Llavall, E., Aldega, L., Cantarelli, V., Corrado, S., Gil-Peña, I., Invernizzi, C., Casas, A.M., 2013. On the origin of cleavage in the Central Pyrenees: structural and paleo-thermal study. Tectonophysics 608, 303–318.

Jackson, M., Craddock, J.P., Ballard, M., Van der Voo, R., McCabe, C., 1989. Anhysteretic remanent magnetic anisotropy and calcite strains in Devonian carbonates from the Appalachian Plateau, New York. Tectonophysics 161, 45–53. https://doi.org/10.1016/0040-1951(89)90300-4.

Jelinek, V., 1981. Characterization of the magnetic fabric of rocks. Tectonophysics 79 (3–4), T63–T67.

Kakimoto, K., Takada, S., Haraguchi, Y., Hagihala, M., Torii, S., Kamiyama, T., Mitamura, H., Tokunaga, M., Hatakeyama, A., Katori, H.A., 2021. Magnetism of AlxFe2−xGeO5 with andalusite structure. J. Phys. Soc. Jpn. 91 (5), 054704. https://doi.org/10.7566/JPSJ.91.054704.

Kissel, C., Barrier, E., Laj, C., Lee, T.Q., 1986. Magnetic fabric in 'undeformed' marine clays from compressional zones. Tectonics 5, 769–781. https://doi.org/10.1029/TC005i005p00769.

Kontny, A., de Wall, H., Sharp, T.G., Pósfai, M., 2000. Mineralogy and magnetic behavior of pyrrhotite from a 260 C section at the KTB drilling site, Germany. Am. Mineral. 85 (10), 1416–1427. https://doi.org/10.2138/am-2000-1010.

Lowrie, W., 1990. Identification of ferromagnetic minerals in a rock by coercivity and unblocking temperature properties. Geophys. Res. Lett. 17 (2), 159–162.

Lüneburg, C.M., Lampert, S.A., Lebit, H.D., Hirt, A.M., Casey, M., Lowrie, W., 1999. Magnetic anisotropy, rock fabrics and finite strain in deformed sediments of SW Sardinia (Italy). Tectonophysics 307 (1–2), 51–74.

Mamtani, M.A., Sengupta, P., 2010. Significance of AMS analysis in evaluating superposed folds in quartzites. Geol. Mag. 147 (6), 910–918. https://doi.org/10.1017/S0016756810000397.

Martínez-Catalán, J.R., Arenas, R., Abati, J., Sánchez-Martínez, S., Díaz-García, F., Fernández-Suárez, J., González-Cuadra, P., Castiñeiras, P., Gómez-Barreiro, J., Díez-Montes, A., González-Clavijo, E., Rubio-Pascual, F.J., Andonaegui, P., Jeffries, T.E., Alcock, J.E., Díaz-Fernández, R., López-Carmona, A., 2009. A rootless suture and the loss of the roots of a Mountain chain: the Variscan belt of NW Iberia. Comptes Rendus Geosciencie 314 (2–3), 114–126.

Martínez-Peña, M.B., Casas-Sainz, A.M., 2003. Cretaceous–tertiary tectonic inversion of the Cotiella Basin (Southern Pyrenees, Spain). Int. J. Earth Sci. 92 (1), 99–113.

Martín-Hernández, F., Dekkers, M.J., Bominaar-Silkens, I.M.A., Maan, J.C., 2008. Magnetic anisotropy behaviour of pyrrhotite as determined by low- and high-field experiments. Geophys. J. Int. 174, 42–54.

Mattauer, M., 1968. Les traits structuraux essentiels de la chaîne pyrénéenne. Rev Géogr Phys Géol Dyn. Rev. Geogr. Phys. Geol. Dyn. 10 (1), 3–12.

Matte, P., 2002. Les plis hercyniens kilométriques couchés vers l'ouest-sud-ouest dans la région du pic du Midi d'Ossau–col du Somport (zone axiale des Pyrénées occidentales). Comptes rendus. Géoscience 334 (10), 773–779.

Mattei, M., Sagnotti, L., Faccenna, C., Funiciello, R., 1997. Magnetic fabric of weakly deformed clay-rich sediments in the Italian peninsula: relationship with compressional and extensional tectonics. Tectonophysics 271 (1–2), 107–122.

Mey, P.H.W., 1967. The Geology of the Upper Ribagorzana and Baliera valleys, Central Pyrenees, Spain. Leidse geol. Meded. Leidse Geol. Meded. 41, 153–220.

Moskowitz, B.M., 1981. Methods for estimating curie temperatures of titanomaghemites from experimental Js-T data. Earth Planet Sci. Lett. 53 (1), 84–88.

Muñoz, J.A., 1992. Evolution of a Continental collision belt: ECORS-pyrenees crustal balanced cross-section. In: Thrust Tectonics. Springer, Netherlands, pp. 235–246.

Oliva-Urcia, B., Gil-Peña, I., Soto, R., Samsó, J.M., Antolín, B., Pueyo, E.L., 2018. New insights into asymmetric folding by means of the anisotropy of magnetic susceptibility, Variscan and Pyrenean folds (SW Pyrenees). Studia Geophys. Geod. 62 (2), 291–322. https://doi.org/10.1007/s11200-017-0143-6.

Oliva-Urcia, B., Larrasoaña, J.C., Travé, A., Garcés, M., Sierra-Campos, P., Pueyo, E.L., Calvín, P., 2024. Iron-carbonate concretions with inverse magnetic fabrics; a record of environmental changes in the middle Eocene marine marls of the Southern Pyrenees? J. Iber. Geol. 1–23.

Parés, J.M., 2015. Sixty years of anisotropy of magnetic susceptibility in deformed sedimentary rocks. Front. Earth Sci. 3 (4). https://doi.org/10.3389/feart.2015.00004.

Parés, J.M., van der Pluijm, B.A., 2002a. Phyllosilicate fabric characterization by low-temperature anisotropy of magnetic susceptibility (LT-AMS). Geophys. Res. Lett. 29 (24), 68. https://doi.org/10.1029/2002GL015459, 1.

Parés, J.M., Van Der Pluijm, B.A., 2002b. Evaluating magnetic lineations (AMS) in deformed rocks. Tectonophysics 350 (4), 283–298.

Parés, J.M., van der Pluijm, B.A., Dinarés-Turell, J., 1999. Evolution of magnetic fabrics during incipient deformation of mudrocks (Pyrenees, northern Spain). Tectonophysics 307 (1–2), 1–14. https://doi.org/10.1016/S0040-1951(99)00115-8.

Parés, J.M., van der Pluijm, B.A., 2014. Low-temperature AMS and the quantification of subfabrics in deformed rocks. Tectonophysics 629, 55–62.

Pastor-Galán, D., Groenhof, O., Izquierdo-Llavall, Esther, E., Dinarès-Turell, J., Pueyo, E. L., 2021. Palaeomagnetism from multi-orogenic terranes is 'not a simple game': Pyrenees' Palaeozoic warning. Geophysical Journal Internationa 227 (2), 849–874.

Poblet, J. 1991. Estructura herciniana i alpina del vessant sud de la Zona Axial del Pirineu central. Ph.D. Thesis, University of Barcelona, 604 p.

Pocoví-Juan, A., Pueyo-Anchuela, O., Pueyo, E., Casas-Sainz, A., Román-Berdiel, T., Gil-Imaz, A., Ramajo-Cordero, J., Mochales, T., García-Lasanta, C., Izquierdo Llavall, E., Parés, J.M., Sánchez, E., Soto, R., Oliván, C., Rodríguez-Pintó, A., Oliva-Urcia, B., Villalaín, J.J., 2014. Magnetic fabrics in the Western Central-Pyrenees: an overview. Tectonophysics 629, 303–318. Tectonophysics, 629, 303–318.

Pueyo-Morer, E.L., Millán-Garrido, H., Pocoví-Juan, A., Parés, J.M., 1997. Determination of the folding mechanism by AMS data. Study of the relation between shortening and magnetic anisotropy in the Pico del Aguila anticline (southern Pyrenees). Phys. Chem. Earth 22 (1–2), 195–201.

Pueyo-Anchuela, O., Gil-Imaz, A., Pocoví-Juan, A., 2010. Significance of AMS in multilayer systems in fold-and-thrust belts. A case study from the Eocene turbidites in the southern Pyrenees (spain). Geol. J. 45 (5–6), 544–561.

Raposo, M.I.B., Drukas, C.O., Basei, M.A., 2014. Deformation in rocks from Itajaí basin, Southern Brazil, revealed by magnetic fabrics. Tectonophysics 629, 290–302.

Raposo, M.I.B., 2017. The south Atlantic Ocean opening and its relationship with the dike swarms emplacement of the Ne São Paulo State (Brazil). Latinmag Letters 7.

Roberts, A.P., Cui, Y., Verosub, K.L., 1995. Waspwaisted hysteresis loops: Mineral magnetic characteristics and discrimination of components in mixed magnetic systems. J. Geophys. Res. Solid Earth 100 (89), 17909–17924.

Rochette, P., 1988. Inverse magnetic fabric in carbonate-bearing rocks. Earth Planet Sci. Lett. 90 (2), 229–237. https://doi.org/10.1016/0012-821X(88)90103-3.

Rodríguez-Méndez, L., Cuevas, J., Tubía, J.M., 2013. Geological map of the central Pyrenees between the Tena and Aragon valleys (Huesca). J. Maps 9 (4), 596–603.

Rodríguez-Méndez, L., Cuevas, J., Tubía, J.M., 2016. Post-Variscan basin evolution in the central Pyrenees: insights from the Stephanian–Permian Anayet Basin. C. R. Géosci. 348 (3–4), 333–341.

Román-Berdiel, T., Casas, A.M., Oliva-Urcia, B., Pueyo, E.L., Liesa, C., Soto, R., 2006. The Variscan Millares granite (central Pyrenees): Pluton emplacement in a T fracture of a dextral shear zone. Geodin. Acta 19 (3–4), 197–211.

Román-Berdiel, T., Casas, A., Oliva-Urcia, B., Pueyo, E.L., Rillo, C., 2004. The main Variscan deformation event in the Pyrenees: New data from the structural study of the Bielsa granite. J. Struct. Geol. 26, 654–677.

Sayab, M., Miettinen, A., Aerden, D., Karell, F., 2017. Orthogonal switching of AMS axes during type-2 fold interference: insights from integrated X-ray computed tomography, AMS and 3D petrography. J. Struct. Geol. 103, 1–16. https://doi.org/10.1016/j.jsg.2009.03.010.

Schmidt, V., Günther, D., Hirt, A.M., 2006. Magnetic anisotropy of calcite at room-temperature. Tectonophysics 418 (1–2), 63–73.

Schwarz, E.J., Vaughan, D.J., 1972. Magnetic phase relations of pyrrhotite. Journal of geomagnetism and geoelectricity. J. Geomagn. Geoelectr. 24 (4), 441–458.

Soto, R., Casas-Sainz, A.M., Oliva-Urcia, B., Román-Berdiel, T., 2022. Guía rápida para el estudio de rocas deformadas a partir del análisis de la Anisotropía de la Susceptiblidad Magnética (ASM). Rev. Soc. Geol. Espana 35 (1), 56–70. https://doi.org/10.55407/rsge.94884.

Teixell, A., 1996. The Ansó transect of the southern Pyrenees: basement and cover thrust geometries. Journal of the Geological Society, London 153 (2), 301–310.

Zwart, H.J., 1963. The structural evolution of the Paleozoic of the Pyrenees. Geol. Rundschau 53, 170–205.

Zwart, H.J., 1979. The Geology of the Central Pyrenees. Leidse Geol. Meded. 50 (1), 74.